Identification of Nonlinear Wave Forces. Part II. Frequency-Domain Analysis

K Worden, P K Stansby and G R Tomlinson
Department of Engineering
University of Manchester
Oxford Road
Manchester
M13 9PL

S A Billings
Department of Automatic Control and Systems Engineering
University of Sheffield
P O Box 600
Mappin Street
Sheffield
S1 4DU

Research Report No 442

October 1991

Identification of Nonlinear Wave Forces. Part II. Frequency-Domain Analysis.

K.Worden, P.K.Stansby and G.R.Tomlinson
Department of Engineering
The University
Oxford Road
Manchester M13 9PL

S.A.Billings
Department of Automatic Control and Systems Engineering
University of Sheffield
Mappin Street
Sheffield S1 3JD

Abstract

In part I of this study, concerned with time-domain results, a number of NARMAX time-series models were obtained for a range of situations of wave loading on slender cylinders. The dual frequency-domain approach is pursued here. First, a review is given of the basic theory of the Volterra expansion for nonlinear systems. The associated higher order Frequency Response Functions (FRF's) are presented. The means of constructing them by the method of harmonic probing is outlined and their interpretation is discussed. A study is made of the higher order FRF's for the Morison equation and a proposed extension, the Morison-Duffing equation. Finally, the FRF's for the aforementioned NARMAX models are determined; it is shown that the fluid systems exhibit a consistent structure in their higher order responses which is not predicted by Morison's equation.

1 Introduction

In a previous paper [1], NARMAX nonlinear time-series methods were applied to experimental force and velocity data for various flows around a cylinder, the object being to obtain mathematical models which would allow accurate prediction of fluid-loading forces from measured instantaneous flow velocities. The situations represented ranged from planar oscillatory flow in a U-tube to a random directional sea.

The standard means of predicting wave forces at present is to use Morison's equation [2].

$$F(t) = \frac{1}{2}\rho D C_d u|u| + \frac{1}{4}\pi\rho D^2 C_m \dot{u} \tag{1}$$

where $F(t)$ is the force per unit axial length on the cylinder, $u(t)$ is the instantaneous flow velocity, ρ is water density and D is the diameter. C_d and C_m are the dimensionless drag and inertia coefficients respectively. In all the cases considered in [1], the NARMAX models gave substantial improvements over the predictions obtained from the Morison equation. (In a separate paper [3], additional terms were added which had a physical interpretation and gave good curve-fits but *not* predictions. This analysis enabled improved force classification into drag, inertia and *history* components.) However, these improvements were obtained at the expense of including extra model terms which had no clear physical interpretation. Further, in the analysis of the U-tube data from an experiment by Obasaju [4], different model structures were obtained for different values of Keulegan-Carpenter number KC, where $KC = U_0 T/D$, for the flows. One reason why this situation might occur is that the discrete-time representation of a continuous-time system is not unique. In order to draw any conclusions from the NARMAX results given in [1] in the time-domain, it is necessary to recover the underlying continuous-time model or use some other means which can reveal any common underlying physical structure in the NARMAX models. This can be done by passing to the frequency- domain where the system has a representation by a number of frequency response functions (FRF's) which can be determined directly from the NARMAX representation [6]. The calculation of the nonlinear FRF's is based on the Volterra series representation of nonlinear systems [5], which has been applied with success to a number of problems in control engineering and structural dynamics in recent years.

The layout of the paper is as follows: section 2 provides a brief introduction to the Volterra representation of a nonlinear system. Section 3 describes how one can obtain the higher order frequency response functions from the system equation of motion (or its NARMAX representation) using the method of harmonic probing. Section 4 is concerned with the validation and interpretation of the higher order FRF's. The harmonic probing procedure is applied in Section 5 to Morison's equation. Finally in Section 6, the higher order FRF's for the NARMAX models from [1] are obtained and it is shown that they exhibit a number of common features.

The results presented in the next two sections are not original. However, as the determination of higher order FRF's by harmonic probing is unlikely to be a well known technique within the context of fluid loading calculations, a review is given in order to make the paper essentially self-contained.

2 The Volterra Series and Higher Order Frequency Response Functions.

The primary problem of system identification is to obtain a mathematical model of a given physical system from consideration of measured input and output data. In general mathematical terms, a system S can be regarded as a *functional* which maps given input functions e.g. $x(t)$, to associated output functions $y(t)$.

$$y(t) = S[x(t)] \tag{2}$$

This is far too general to be very illuminating. However, it is well known that the input-output functional for a linear system can always be written in the form

$$y(t) = \int d\tau h(\tau - t)x(\tau) \tag{3}$$

a relationship which is sometimes referred to as Duhamel's integral. Within this framework, the system is specified uniquely by its Green's function or impulse response function $h(t)$. The Fourier transform $\mathcal{F}$ of equation (3) yields the familiar frequency domain expression

$$Y(\omega) = H(\omega)X(\omega) \tag{4}$$

where $X(\omega)$ and $Y(\omega)$ are the Fourier transforms of $x(t)$ and $y(t)$ respectively and $H(\omega) = \mathcal{F}[h(t)]$ is the system Frequency Response Function or FRF. All information about the system is encoded in either of the functions $h(t)$ and $H(\omega)$. Which representation is used in a given problem will usually be dictated by the form of the answer required. In vibration problems, the frequency domain approach is usually adopted; displaying the FRF $H(\omega)$ shows immediately those frequencies at which large outputs can be expected i.e. peaks in $H(\omega)$ corresponding to the system resonances.

Equations (3) and (4) are manifestly linear and therefore cannot hold for arbitrary nonlinear systems. However, both admit a generalisation. The extended form of equation (3) was obtained in the early part of this century by Volterra [7]. It takes the form of an infinite series

$$y(t) = y_1(t) + y_2(t) + y_3(t) + \dots \tag{5}$$

where

$$y_1(t) = \int_{-\infty}^{+\infty} d\tau h_1(\tau)x(t - \tau) \tag{6}$$

$$y_2(t) = \int_{-\infty}^{+\infty}\int_{-\infty}^{+\infty} d\tau_1 d\tau_2 h_2(\tau_1, \tau_2)x(t - \tau_1)x(t - \tau_2) \tag{7}$$

$$y_3(t) = \int_{-\infty}^{+\infty}\int_{-\infty}^{+\infty}\int_{-\infty}^{+\infty} d\tau_1 d\tau_2 d\tau_3 h_2(\tau_1, \tau_2, \tau_3)x(t - \tau_1)x(t - \tau_2)x(t - \tau_3) \tag{8}$$

The form of the general term is obvious from the above. The functions $h_1(\tau)$, $h_2(\tau_1, \tau_2)$, $h_3(\tau_1, \tau_2, \tau_3)$, $\dots$ $h_n(\tau_1, \dots, \tau_n)$, $\dots$ are generalisations of the linear impulse response function and are ususally referred to as *Volterra kernels*. The use of the Volterra series in dynamics stems from the seminal paper of Barrett [8] in which the series was applied to nonlinear differential equations for the first time. One can think of the series as a generalisation of the Taylor series from functions to functionals. The expression (3) simply represents the lowest order truncation which is of course exact only for linear systems.

It can be shown [5] that the kernels can be considered to be symmetric without loss of generality i.e. $h_2(\tau_1, \tau_2) = h_2(\tau_2, \tau_1)$ etc.

As stated above, there exists a dual frequency-domain representation for nonlinear systems. The *higher order FRF's* or *Volterra kernel transforms* $H_n(\omega_1, \dots, \omega_n)$, $n = 1, \dots, \infty$ are defined as the multi-dimensional Fourier transforms of the kernels, i.e.

$$H_n(\omega_1,\ldots,\omega_n) = \int_{-\infty}^{+\infty}\cdots\int_{-\infty}^{+\infty} d\tau_1\ldots d\tau_n h_n(\tau_1,\ldots,\tau_n)e^{-i(\omega_1\tau_1+\ldots+\omega_n\tau_n)} \quad (9)$$

$$h_n(\tau_1,\ldots,\tau_n) = \frac{1}{(2\pi)^n}\int_{-\infty}^{+\infty}\cdots\int_{-\infty}^{+\infty} d\omega_1\ldots d\omega_n H_n(\omega_1,\ldots,\omega_n)e^{+i(\omega_1\tau_1+\ldots+\omega_n\tau_n)} \quad (10)$$

It is a simple matter to show that symmetry of the kernels implies symmetry of the kernel transforms so for example, $H_2(\omega_1,\omega_2) = H_2(\omega_2,\omega_1)$.

It is then a straightforward matter (Appendix A) to obtain the frequency-domain dual of the expression (5)

$$Y(\omega) = Y_1(\omega) + Y_2(\omega) + Y_3(\omega) + \ldots \quad (11)$$

where

$$Y_1(\omega) = H_1(\omega)X(\omega) \quad (12)$$

$$Y_2(\omega) = \frac{1}{2\pi}\int_{-\infty}^{+\infty} d\omega_1 H_2(\omega_1,\omega-\omega_1)X(\omega_1)X(\omega-\omega_1) \quad (13)$$

$$Y_3(\omega) = \frac{1}{(2\pi)^2}\int_{-\infty}^{+\infty}\int_{-\infty}^{+\infty} d\omega_1 d\omega_2 H_3(\omega_1,\omega_2,\omega-\omega_1-\omega_2)X(\omega_1)X(\omega_2)X(\omega-\omega_1-\omega_2) \quad (14)$$

The remainder of this paper is concerned with the determination and interpretation of the higher order FRF's. As for a linear system, the choice of time or frequency-domain representation is largely dictated by the problem. In this case, the frequency-domain is indicated for the following reason. The objects under study are NARMAX difference equation models for a number of different fluid-loading systems obtained in [1]. It was observed there that time-domain models for two similar flows (i.e. two flows in a U-tube differing only in their Keulegan-Carpenter number) might contain different model terms. Because the NARMAX representation of a system is not unique, one cannot be sure if differences in the model structures for different flows are due to differences in the underlying physics or simply a reflection of the non-uniqueness. However, the non-uniqueness is not a problem in the frequency-domain. No matter what the form of the model, if it represents the measured data accurately it must reflect the correct frequency content, both from linear and nonlinear parts of the system. In other words, although there may be a number of discrete-time models which represent a continuous-time system to a given order of accuracy, and these models can differ in structure; the higher-order FRF's corresponding to the discrete models must all agree with those for the continuous system and with each other. This will be discussed further in Section 4.

3 Harmonic Probing of the Volterra series.

The subject of this section is a method of determining the higher order FRF's for a system. If one has measured input and output time data, it is possible to evaluate the

FRF's by carrying out many multi-dimensional Fast Fourier Transforms and averaging the results, in much the same way as one would evaluate a standard linear transfer function [9]. However, this approach requires that the input be a Gaussian white noise sequence; also, the computational burden of carrying out multi-dimensional FFT's makes evaluation of FRF's higher than second order prohibitive by this method. Alternatively, it is possible to estimate the higher order FRF's efficiently by harmonic testing of a system [10].

If one knows the equation of motion of a system, an alternative approach can be used which yields exact expressions for the higher order FRF's. The method of harmonic probing was introduced by Bedrossan and Rice in [11] specifically for systems with continuous-time equations of motion. The method was extended to discrete-time systems by Billings and Tsang in [6]. An alternative, recursive approach to probing is presented in [12].

A review of the method of harmonic probing will now be presented. In order to explain how the procedure works, it is necessary to determine how a system responds to a harmonic or periodic input in terms of its Volterra series.

First consider a periodic excitation composed of a single harmonic

$$x(t) = e^{i\Omega t} \tag{15}$$

The spectral representation of this function follows from the representation of the δ function given in Appendix A.

$$X(\omega) = 2\pi\delta(\omega - \Omega) \tag{16}$$

Substituting this expression into equations (12) to (14) and forming the total response as in (11) yields, up to third order,

$$Y(\omega) = H_1(\omega).2\pi\delta(\omega - \Omega) +$$

$$\frac{1}{2\pi}\int_{-\infty}^{+\infty} d\omega_1 H_2(\omega_1, \omega - \omega_1).2\pi\delta(\omega_1 - \Omega).2\pi\delta(\omega - \omega_1 - \Omega) +$$

$$\frac{1}{(2\pi)^2}\int_{-\infty}^{+\infty}\int_{-\infty}^{+\infty} d\omega_1 d\omega_2 H_3(\omega_1, \omega_2, \omega - \omega_1 - \omega_2).$$

$$2\pi\delta(\omega_1 - \Omega).2\pi\delta(\omega_2 - \Omega).2\pi\delta(\omega - \omega_1 - \omega_2 - \Omega) + \ldots \tag{17}$$

using the argument-changing property of the delta function and carrying out the integrals gives

$$Y(\omega) = 2\pi\{H_1(\Omega)\delta(\omega - \Omega) + H_2(\Omega, \Omega)\delta(\omega - 2\Omega) + H_3(\Omega, \Omega, \Omega)\delta(\omega - 3\Omega) + \ldots \tag{18}$$

Taking the inverse Fourier transform yields the required response,

$$y(t) = H_1(\Omega)e^{i\Omega t} + H_2(\Omega, \Omega)e^{i2\Omega t} + H_3(\Omega, \Omega, \Omega)e^{i3\Omega t} + \ldots \tag{19}$$

This shows clearly that one should expect components in the output at multiples of the excitation frequency, i.e. harmonics. The important point here is that the component in the output at the forcing frequency is $H_1(\Omega)$.

Probing the system with a single harmonic only yields information about the values of the FRF's on the diagonal line in the frequency space. In order to obtain further information one should use multi-frequency excitations. With this in mind, consider the 'two-tone' input

$$x(t) = e^{i\Omega_1 t} + e^{i\Omega_2 t} \tag{20}$$

which has spectral representation

$$X(\omega) = 2\pi\delta(\omega - \Omega_1) + 2\pi\delta(\omega - \Omega_2) \tag{21}$$

substituting into (12)-(14) and thence into (11) yields

$$Y(\omega) = H_1(\omega).2\pi\delta(\omega - \Omega_1) + H_1(\omega).2\pi\delta(\omega - \Omega_2) +$$

$$\frac{1}{2\pi}\int_{-\infty}^{+\infty} d\omega_1 H_2(\omega_1, \omega - \omega_1).$$

$$\{2\pi\delta(\omega_1 - \Omega_1) + 2\pi\delta(\omega_1 - \Omega_2)\}\{2\pi\delta(\omega - \omega_1 - \Omega_1) + 2\pi\delta(\omega - \omega_1 - \Omega_2)\} +$$

$$\frac{1}{(2\pi)^2}\int_{-\infty}^{+\infty}\int_{-\infty}^{+\infty} d\omega_1 d\omega_2 H_3(\omega_1, \omega_2, \omega - \omega_1 - \omega_2).$$

$$\{2\pi\delta(\omega_1 - \Omega_1) + 2\pi\delta(\omega_1 - \Omega_2)\}.\{2\pi\delta(\omega_2 - \Omega_1) + 2\pi\delta(\omega_2 - \Omega_2)\}.$$

$$\{2\pi\delta(\omega - \omega_1 - \omega_2 - \Omega_1) + 2\pi\delta(\omega - \omega_1 - \omega_2 - \Omega_2)\} + \ldots \tag{22}$$

It is a straightforward but tedious matter to expand this expression and perform the integrals. After making use of the symmetry properties of the higher order FRF's, one obtains

$$\frac{Y(\omega)}{2\pi} = H_1(\Omega_1)\delta(\omega - \Omega_1) + H_1(\Omega_2)\delta(\omega - \Omega_2) +$$

$$H_2(\Omega_1, \Omega_1)\delta(\omega - 2\Omega_1) + 2H_2(\Omega_1, \Omega_2)\delta(\omega - \Omega_1 - \Omega_2) + H_2(\Omega_2, \Omega_2)\delta(\omega - 2\Omega_2) +$$

$$H_3(\Omega_1, \Omega_1, \Omega_1)\delta(\omega - 3\Omega_1) + 3H_3(\Omega_1, \Omega_1, \Omega_2)\delta(\omega - 2\Omega_1 - \Omega_2) +$$

$$3H_3(\Omega_1, \Omega_2, \Omega_2)\delta(\omega - \Omega_1 - 2\Omega_2) + H_3(\Omega_2, \Omega_2, \Omega_2)\delta(\omega - 3\Omega_2) + \ldots \tag{23}$$

On taking the inverse Fourier transform, one obtains the response up to third order

$$y(t) = H_1(\Omega_1)e^{it\Omega_1} + H_1(\Omega_2)e^{it\Omega_2} +$$

$$H_2(\Omega_1, \Omega_1)e^{it2\Omega_1} + 2H_2(\Omega_1, \Omega_2)e^{it(\Omega_1+\Omega_2)} + H_2(\Omega_2, \Omega_2)e^{it2\Omega_2} +$$

$$H_3(\Omega_1,\Omega_1,\Omega_1)e^{it3\Omega_1} + 3H_3(\Omega_1,\Omega_1,\Omega_2)e^{it(2\Omega_1+\Omega_2)} +$$

$$3H_3(\Omega_1,\Omega_2,\Omega_2)e^{it(\Omega_1+2\Omega_2)} + H_3(\Omega_2,\Omega_2,\Omega_2)e^{it3\Omega_2} + \ldots \tag{24}$$

The important thing to note here is that the amplitude of the component at the *sum* frequency for the excitation i.e. at $\Omega_1 + \Omega_2$ is twice the second order FRF $H_2(\Omega_1,\Omega_2)$. In fact, if a general periodic excitation is used i.e.

$$x(t) = e^{i\Omega_1 t} + \ldots + e^{i\Omega_n} \tag{25}$$

it is not difficult to show that the amplitude of the output component at the frequency $\Omega_1 + \ldots + \Omega_n$ is $n!H_n(\Omega_1,\ldots,\Omega_n)$. This single fact is the basis of the harmonic probing algorithm. In order to find the second order FRF of a system for example, one substitutes the expressions for the input (20) and general output (24) into the system equation of motion and extracts the coefficient of $e^{it(\Omega_1+\Omega_2)}$; this yields an algebraic expression for H_2.

The procedure is best illustrated by choosing a concrete example. Consider the continuous-time system.

$$Dy + y + y^2 = x(t) \tag{26}$$

where $D = \frac{d}{dt}$. In order to find H_1, one substitutes in the equation, the probing expressions

$$x(t) = x_1^p(t) = e^{i\Omega t} \tag{27}$$

$$y(t) = y_1^p(t) = H_1(\Omega)e^{i\Omega t} \tag{28}$$

The result being

$$(i\Omega + 1)H_1(\Omega)e^{i\Omega t} + H_1(\Omega)^2 e^{i2\Omega t} = e^{i\Omega t} \tag{29}$$

equating the coefficients of $e^{i\Omega t}$ on each side of this expression yields an equation for H_1

$$(i\Omega + 1)H_1(\Omega) = 1 \tag{30}$$

which is trivially solved, yielding the expression

$$H_1(\Omega) = \frac{1}{i\Omega + 1} \tag{31}$$

Evaluation of H_2 is only a little more complicated. One substitutes the probing expressions

$$x(t) = x_2^p(t) = e^{i\Omega_1 t} + e^{i\Omega_2 t} \tag{32}$$

$$y(t) = y_2^p(t) = H_1(\Omega_1)e^{i\Omega_1 t} + H_1(\Omega_2)e^{i\Omega_2 t} + 2H_2(\Omega_1,\Omega_2)e^{i(\Omega_1+\Omega_2)t} \tag{33}$$

Note that in passing from the general output (24) to the probing expression (33), all second order terms except that at the sum frequency have been deleted. This is a very useful simplification and is allowed because no combination of the missing terms

can produce a component at the sum frequency and therefore they cannot appear in the final expression for H_2. Substituting (32) and (33) into (26), and extracting the coefficients of $e^{i(\Omega_1+\Omega_2)t}$ yields

$$\{i(\Omega_1+\Omega_2)+1\}H_2(\Omega_1,\Omega_2)+H_1(\Omega_1)H_1(\Omega_2)=0 \tag{34}$$

So that

$$H_2(\Omega_1,\Omega_2)=\frac{-H_1(\Omega_1)H_1(\Omega_2)}{i(\Omega_1+\Omega_2)+1}$$

$$=-H_1(\Omega_1)H_1(\Omega_1)H_1(\Omega_1+\Omega_2)$$

$$=\frac{-1}{(i\Omega_1+1)(i\Omega_2+1)(i[\Omega_1+\Omega_2]+1)} \tag{35}$$

on using the previously obtained expression for H_1.

The next example is a little more interesting; consider the following version of Duffing's equation for a nonlinear oscillator

$$mD^2y+cDy+ky+k_2y^2+k_3y^3=x(t) \tag{36}$$

H_1 and H_2 for this system can be evaluated by exactly the same procedure as used on the previous example. The results being

$$H_1(\omega)=\frac{1}{-m\omega^2+ic\omega+k} \tag{37}$$

$$H_2(\omega_1,\omega_2)=-\frac{k_2}{2}H_1(\omega_1)H_1(\omega_2)H_1(\omega_1+\omega_2) \tag{38}$$

Note that the constant k_2 multiplies the whole expression for H_2, so that if the square-law term is absent from the equation of motion, H_2 vanishes. This reflects a quite general property of the Volterra series; if all nonlinear terms in the equation of motion for a system are odd powers of x or y, then the associated Volterra series has no even order kernels. As a consequence it will possess no even order kernel transforms.

In order to obtain H_3, the required probing expressions are

$$x(t)=x_3^p(t)=e^{i\omega_1 t}+e^{i\omega_2 t}+e^{i\omega_3 t} \tag{39}$$

$$y(t)=y_3^p(t)=H_1(\omega_1)e^{i\omega_1 t}+H_1(\omega_2)e^{i\omega_2 t}+H_1(\omega_3)e^{i\omega_3 t}$$

$$+2H_2(\omega_1,\omega_2)e^{i(\omega_1+\omega_2)t}+2H_2(\omega_1,\omega_3)e^{i(\omega_1+\omega_3)t}+2H_2(\omega_2,\omega_3)e^{i(\omega_2+\omega_3)t}$$

$$+6H_3(\omega_1,\omega_2,\omega_3)e^{i(\omega_1+\omega_2+\omega_3)t} \tag{40}$$

which are sufficiently general to obtain H_3 for any system. Substituting into the Duffing equation and extracting the coefficient of $e^{i(\omega_1+\omega_2+\omega_3)t}$ yields,

$$H_3(\omega_1,\omega_2,\omega_3)=-\frac{1}{6}H_1(\omega_1+\omega_2+\omega_3).$$

$$\{4k_2\left(H_1(\omega_1)H_2(\omega_2,\omega_3)+H_1(\omega_2)H_2(\omega_3,\omega_1)+H_1(\omega_3)H_2(\omega_1,\omega_2)\right)+k_3H_1(\omega_1)H_1(\omega_2)H_1(\omega_3)\} \tag{41}$$

It is a general property of systems that all higher order FRF's can be expressed in terms of H_1 for the system. The exact form of the expression will of course depend on the particular system.

A discussion of the interpretation of these functions is deferred until the next section.

The harmonic probing algorithm has been established above for all continuous-time systems i.e. those whose evolution is governed by differential equations of motion. The NARMAX models which shall be analysed later are difference equations so the probing algoritm requires a little modification [6]. Consider the difference equation analogue of equation (26)

$$\Delta y + y + y^2 = x(t) \tag{42}$$

where Δ is the backward shift operator, defined by $\Delta z(t) = z(t-1)$. (Throughout this paper it is assumed, except where indicated that the sampling interval for a discrete-time system is scaled to unity. This yields a unit sampling frequency and Nyquist frequency of 0.5). In the usual notation for difference equations, (42) becomes

$$y_{i-1} + y_i + y_i^2 = x_i \tag{43}$$

However, the form containing Δ allows the most direct comparison with the continuous-time case. It is clear from the above that the only differences for harmonic probing of discrete-time systems will be generated by the fact that the operator Δ has a different action on functions $e^{i\omega t}$ to the operator D. This action is very simple to compute,

$$\Delta\, e^{i\omega t} = e^{i\omega(t-1)} = e^{-i\omega}.e^{i\omega t} \tag{44}$$

It is amusing to note that this action follows from the fact that $\Delta = e^{-D}$ as an operator equation; as $e^{i\omega t}$ is an eigenfunction of D with eigenvalue $i\omega$, it is also an eigenfunction of Δ with eigenvalue $e^{-i\omega}$. It is now clear that one can carry out the harmonic probing algorithm for (42) exactly as for the continuous-time (26), the only difference will be that the Δ operator will generate a multiplier $e^{-i\omega}$ everywhere that D generated a factor $i\omega$. As a consequence H_1 and H_2 for (42) are easily computed.

$$H_1(\omega) = \frac{1}{e^{-i\omega}+1} \tag{45}$$

$$H_2(\omega_1,\omega_2) = \frac{-H_1(\omega_1)H_1(\omega_2)}{e^{-i(\omega_1+\omega_2)}+1}$$

$$= -H_1(\omega_1)H_1(\omega_1)H_1(\omega_1+\omega_2) \tag{46}$$

Note that the form of H_2 as a function of H_1 is identical to that for the continuous-time system.

It is possible at this point to make a quite general statement. Given a continuous-time system with linear or nonlinear equation of motion $f(D,y,x) = 0$ and higher order FRF's $H_n^c(\omega_1,\ldots,\omega_n), n = 1,\ldots,\infty$, the corresponding discrete-time system

$f(\Delta, y, x) = 0$ has higher order FRF's $H_n^d(\omega_1, \ldots, \omega_n) = H_n^c(-ie^{-i\omega_1}, \ldots, -ie^{-i\omega_n}), n = 1, \ldots, \infty$. Further the functional relationships between the H_n and H_1 will be identical in both cases.

The system in equation (42) is not a NARMAX system as it is a nonlinear function of the most recent sampled value y_i. A NARMAX model has the general form [1]

$$y_i = F(y_{i-1}, \ldots, y_{i-n_y}; x_{i-1}, \ldots, x_{i-n_x}) \tag{47}$$

The relevant existence theorems [13] [14] show that this form is general enough to represent almost all input-output systems.

4 Validation and Interpretation of the Higher Order Frequency Response Functions.

In order to justify studying the higher order FRF's it is necessary to show that they contain useful information about whatever system is under examination. In fact, as time and frequency-domain representations are completely equivalent, the higher order FRF's contain *all* system information; later in this section it is demonstrated that important facts can be conveyed in a very direct and visible way.

Before discussing matters of interpretation it is important to address the question of uniqueness of the higher order FRF's as the analysis of the final section of this paper is predicated on the assumption that the non-uniqueness of the time-domain NARMAX representation of a system does not necessarily affect the frequency-domain representation.

The first thing which must be established is the correspondence between the FRF's of the continuous system and the FRF's of the discrete approximations. Consider the Duffing oscillator of equation (36); a discrete-time representation for this system could be obtained by adopting discrete approximations to the derivatives. The coarsest approximation available is the forward-difference approximation in which

$$\dot{y}_i \approx \frac{y_i - y_{i-1}}{\Delta t} \tag{48}$$

$$\ddot{y}_i \approx \frac{y_{i+1} - 2y_i + y_{i-1}}{\Delta t^2} \tag{49}$$

where Δt is the sampling interval. Substituting these expressions into (36) with the coefficient values given above, yields the NARMAX representation

$$y_i = \left\{\frac{2 + c\Delta t + k\Delta t^2}{1 + c\Delta t}\right\} y_{i-1} - \left\{\frac{1}{1 + c\Delta t}\right\} y_{i-2}$$

$$- \left\{\frac{k_2\Delta t^2}{1 + c\Delta t}\right\} y_{i-1}^2 - \left\{\frac{k_3\Delta t^2}{1 + c\Delta t}\right\} y_{i-1}^3 + \left\{\frac{\Delta t^2}{1 + c\Delta t}\right\} x_{i-1} \tag{50}$$

In fact, because this is based on the coarse approximations (48) and (49) it does not yield good representations of the higher order FRF's. In order to demonstrate accurate FRF's from a NARMAX model, the following numerical simulation was carried out. A fourth-order Runge-Kutta scheme was used to obtain the response of the system (36) under excitation by a Gaussian noise sequence $x(t)$ with rms 10.0 and frequency range 0 to 90 Hz. The coefficient values adopted were: $m = 1, c = 20, k = 10^4, k_2 = 10^7, k_3 = 5.10^9$. This system has a resonant frequency of

$\omega_r = \sqrt{k/m} = 99 rad/s$ or $f_r = \frac{\omega_r}{2\pi} = 15.75 Hz$. The data was generated with a sampling interval of 0.005 seconds, giving a Nyquist frequency of 100 Hz.

A NARMAX model was fitted to 1000 points of the resulting discrete x and y data using the estimation and validation methods described in [1]. The result was

$$\begin{aligned} y_i &= 1.6696 y_{i-1} - 0.90348 y_{i-2} \\ &- 2.1830 \times 10^2 y_{i-1}^2 - 1.0665 \times 10^5 y_{i-1}^3 \\ &+ 3.0027 \times 10^{-6} u_i + 1.8040 \times 10^{-5} u_{i-1} \\ &+ 2.7676 \times 10^{-6} u_{i-2} \end{aligned} \tag{51}$$

Figure 1 shows a comparison between the original y data from the simulation, and that predicted by the NARMAX model (51), when excited by the same input data x; the NARMAX model clearly gives a good representation of the system in the time-domain. The fitted model was then used to generate the higher order FRF's H_1, H_2 and H_3 by the method of harmonic probing. As the exact results could also be obtained by harmonic probing of (36), direct comparisons could be made. In all cases, the exact FRF's are given with the frequency scale in Hz; the FRF's for the discrete model are given with normalised frequency scales $f_n = f/f_s$ where f_s is the sampling frequency, the Nyquist frequency is 0.5 in these units.

Figure 2 shows a comparison between the exact H_1 and that obtained from the model, the agreement is excellent. However, an important point must be raised here. H_1 for the discrete system is only an approximation to H_1 for the continuous system up to the Nyquist frequency of 0.5 (100 Hz); it is only plotted up to this frequency in Figures 2c and 2d because it simply repeats beyond this point and is therefore meaningless.

The comparison between the exact H_2 and that from the NARMAX model is given in Figure 3, the same comparison using the contour maps for the functions is shown in Figure 4; again the agreement is very good. Note that because H_2 contains factors $H_1(2\pi f_1)$ and $H_2(2\pi f_2)$ it would meaningless to plot it outside the ranges corresponding to $f_1 \leq 100, f_2 \leq 100$. Further, H_2 also contains a factor $H_1(2\pi(f_1+f_2))$ so that the plots should not extend past the area specified by $f_1+f_2 \leq 100$. Rather than plot irregular shaped regions, the H_2 figures presented in this paper include information beyond this last bound, which is indicated by the solid line in the model contour maps in Figure 4; information presented outside this region on any H_2 plot should not be regarded as meaningful.

The comparison between the exact H_3 and model H_3 is given in Figure 5, and in contour map form in Figure 6. Unfortunately, the whole H_3 surface cannot be plotted as it exists as a three-dimensional manifold embedded in a four-dimensional space over the $(\omega_1, \omega_2, \omega_3)$ 'plane'. However, one can plot two-dimensional submanifolds of H_3, and this is the approach which is usually adopted. Figures 6 and 7 show $H_3(\omega_1, \omega_2, \omega_1)$ plotted over the (ω_1, ω_2) plane. The region of validity of the H_3 surface is a little more complicated in this case, and is shown on the model H_3 contour maps in Figures 7c and 7d.

In all cases, agreement between the exact H_n and those obtained from the NARMAX model is impressive. For a less passive comparison, Figure 8 shows the gain and phase of the output components y_1, y_2 and y_3 obtained from the systems defined by the exact and model FRF's when excited by a unit sinusoid at various frequencies. Again, agreement is excellent.

Having established that a NARMAX model can yield good representations of the FRF's from a continuous system, the next question which must be addressed concerns the correspondence between frequency-domain representations of different

yet *exactly* equivalent NARMAX models. (Non-uniqueness is actually a problem with most methods of modelling, it is not specific to NARMAX). Suppose one has obtained as an accurate discretisation of a continuous system, the NARMAX model

$$y_i = a_1 y_{i-1} + a_2 y_{i-2} + b_1 x_{i-1} \tag{52}$$

As this expression holds for all values of i (away from the initial points), it can just as well be written as

$$y_{i-1} = a_1 y_{i-2} + a_2 y_{i-3} + b_1 x_{i-2} \tag{53}$$

Substituting (53) into (52) yields the NARMAX model

$$y_i = (a_1^2 + a_2) y_{i-2} + a_1 a_2 y_{i-3} + b_1 x_{i-1} + b_1 x_{i-2} \tag{54}$$

which is exactly equivalent to (52) yet contains different terms. This type of ambiguity will occur for any system which regresses the present output onto past values of output. It is a reflection of a type of ambiguity for continuous-time systems; one can always differentiate the equation of motion to obtain a completely equivalent system. The only thing which changes is the set of objects for which initial conditions are required. Harmonic probing of (52) yields (in symbolic notation where $\Delta = e^{-i\omega}$)

$$H_1^{(52)} = \frac{b_1 \Delta}{1 - a_1 \Delta - a_2 \Delta^2} \tag{55}$$

while probing of (54) gives the superficially different

$$H_1^{(54)} = \frac{b_1 \Delta + a_1 b_1 \Delta^2}{1 - (a_1^2 + a_2) \Delta^2 - a_1 a_2 \Delta^3} \tag{56}$$

However, the latter expression factors

$$H_1^{(54)} = \frac{b_1 \Delta (a_1 \Delta + 1)}{(a_1 \Delta + 1)(1 - a_1 \Delta - a_2 \Delta^2)} = \frac{b_1 \Delta}{1 - a_1 \Delta - a_2 \Delta^2} = H_1^{(52)} \tag{57}$$

The final type of non-uniqueness is generated by the fact that NARMAX models can be approximately equivalent. As an illustration consider the simple system

$$y_i = \alpha y_{i-1} + x_{i-1} \tag{58}$$

If α is small, a simple application of the binomial theorem gives

$$(1 - \alpha\Delta) y_i = x_{i-1} \Longrightarrow \quad y_i = (1 - \alpha\Delta)^{-1} x_{i-1} \Longrightarrow \quad y_i = (1 + \alpha\Delta) x_{i-1} + O(\alpha^2)$$

So the system

$$y_i = x_{i-1} + \alpha x_{i-2} \tag{59}$$

is equivalent to the system in (59) up to $O(\alpha^2)$. Now, harmonic probing of system (58) gives yields the FRF

$$H_1^{(58)}(\omega) = \frac{1}{1 - \alpha e^{-i\omega}} \tag{60}$$

and a similar analysis for (59) gives

$$H_1^{(60)}(\omega) = 1 + \alpha e^{-i\omega} = \frac{1}{1 - \alpha e^{-i\omega}} + O(\alpha) = H_1^{(58)}(\omega) + O(\alpha) \tag{61}$$

Note that by retaining n terms in the binomial expansion above, the model

$$y_i = x_{i-1} + \alpha x_{i-2} + \ldots + \alpha^{n-1} x_{i-n}$$

is obtained which is equivalent to (58) up to $O(\alpha^n)$. As a result, the system (58) can be be represented with arbitrary accuracy by the expansion above if n is taken large enough. However, note that one representation has only three model terms while the other has n with n possibly large. This serves to illustrate why it is important to correctly detect the model structure or which terms are in the model in order to yield a parsimonious model [15].

One must be careful not to regard these simple arguments as generating a general principle; however, it would seem likely that equivalence of two NARMAX models up to a given order of accuracy would imply equivalence of the corresponding FRF's up to the same order of accuracy. This is easy to establish in the case of a general linear system by an extension of the argument above.

The various cases discussed above exhaust all obvious possibilities for obtaining different NARMAX representations of a given system.

This discussion is simply intended as an argument that all NARMAX models which are equivalent in the sense that they furnish a discrete approximation to a continuous system will have higher order FRF's which not only approximate to each other but also to those of the underlying continuous system. It does not constitute a rigorous proof in any sense; however, it is difficult to imagine a situation under which this condition would not hold.

Having established some confidence in their reliability, the interpretation of the higher order FRF's can be discussed. The Duffing oscillator system (36) serves well as an illustration. The magnitude and phase of the expression (37) for $H_1(\omega) = H_1(2\pi f)$ is given in Figures 2a and 2b on the frequency interval 0 to 100 Hz. The interpretation of these figures, traditionally given together and universally called the Bode plot, is well known; the peak in the magnitude at $f = f_r = 15.75Hz$ shows that for this frequency of excitation the amplitude of the linear part of the response $y_1(t)$ is a maximum. The Bode plot thus allows the immediate identification of those excitation frequencies at which the vibration level of the system is likely to be high.

Interpretation of the second order FRF is also straightforward. The magnitude and phase of H_2 for the Duffing system above are given in Figures 3a and 3b (resp. 4a and 4b) as surfaces (resp. contour maps) over the $(f_1, f_2) = (\frac{\omega_1}{2\pi}, \frac{\omega_2}{2\pi})$ plane. The frequency ranges for the plot are the same as for H_1 in Figure 2. A number of ridges are observed. These are in direct correspondence with the peak in H_1 as follows. According to equation (38), H_2 is a constant multiple of $H_1(\omega_1)H_1(\omega_2)H_1(\omega_1+\omega_2)$. As a consequence H_2 possesses local maxima at positions where the H_1 factors have local maxima. Consequently there are two ridges in the H_2 surface corresponding to the lines $\omega_1 = \omega_r = 2\pi f_r$ and $\omega_2 = \omega_r$. These are along lines parallel to the frequency axes. In addition, H_2 has local maxima generated by the $H_1(\omega_1 + \omega_2)$ factor along the line $\omega_1 + \omega_2 = \omega_r$. This ridge has an important consequence; it indicates that one can expect a maximum in the second order output $y_2(t)$ if the system is excited by two sinusoids whose sum frequency is the linear resonant frequency. This shows clearly why estimation of a transfer function by linear methods is inadequate for nonlinear systems; such a transfer function would usually indicate a maximum in the output for a harmonic excitation close to the linear resonant frequency. However, it would fail to predict that one could excite a large nonlinear component in the output by exciting at $\omega = \frac{\omega_r}{2}$; this is a consequence of the trivial decomposition $2e^{i\frac{\omega_r}{2}t} = e^{i\frac{\omega_r}{2}t} + e^{i\frac{\omega_r}{2}t}$ which means that the signal can be regarded as a 'two-tone'

input with a sum frequency at the linear resonance ω_r. The importance of the second order FRF is now clear. It reveals those pairs of excitation frequencies which will conspire to produce large levels of vibration as a result of second order nonlinear effects.

The interpretation of H_3 for the system is very similar. Consideration of equation (41) shows that for a three-tone input of the form (39) one should expect maxima in the third order output $y_3(t)$ if the following conditions are satisfied: $\omega_1 = \omega_r$, $\omega_2 = \omega_r$, $\omega_3 = \omega_r$, $\omega_1 + \omega_2 = \omega_r$, $\omega_2 + \omega_3 = \omega_r$, $\omega_3 + \omega_1 = \omega_r$, $\omega_1 + \omega_2 + \omega_3 = \omega_r$. The presence of these 'combination resonances' would be indicated by the presence of ridges in the H_3 surface. Although Figures 6 and 7 only show the 'projections' of H_3 over the (ω_1, ω_2), they are sufficient to indicate the presence of the 'combination resonances' $\omega_1 = \omega_r$, $\omega_2 = \omega_r$, $\omega_1 + \omega_2 = \omega_r$, $2\omega_1 = \omega_r$, $2\omega_1 + \omega_2 = \omega_r$. It is clear that the local maximum distributions become more and more complex as the order of the FRF increases.

The arguments above show that the higher FRF's provide directly visible information about the possible excitation of large nonlinear vibrations through the cooperation of certain frequencies.

5 Analysis of the Morison Equation.

Having reviewed the appropriate machinery for generating and interpreting higher order FRF's, it can now be applied to Morison's equation. One slight complication arises. In the previous discussion, it has been assumed throughout that the Volterra series for a given system exists. In fact, this need not be the case; a necessary condition for existence is that all nonlinearities must be infinitely differentiable [16]. This condition is not satisfied for Morison's equation because of the drag term $u(t)|u(t)|$ which has a discontinuous second derivative. However, according to the Weierstrass approximation theorem, one can approximate this term by a polynomial to any desired accuracy on a given range; this yields an approximation to Morison's equation for which the Volterra series exists. It is shown in Appendix A of [1] that the best (in the least squared error sense) approximation to $u|u|$ on a symmetric interval $[V, V]$ is given by

$$u|u| = \frac{5V}{16}u + \frac{35}{48V}u^3 + O(u^5) \tag{62}$$

For a regular wave, one would take V to be the maximum velocity, for an irregular wave, the rms velocity could be used. The expression above yields the approximate form for Morison's equation

$$F(t) = \frac{1}{2}\rho D C_d \left\{ \frac{5V}{16}u + \frac{35}{48V}u^3 \right\} + \frac{1}{4}\pi\rho D^2 C_m \dot{u} + O(u^5) \tag{63}$$

or

$$F(t) = K_d^{(1)}u + K_d^{(3)}u^3 + K_m\dot{u} \tag{64}$$

in a convenient shorthand. Application of the harmonic probing algorithm is straightforward and yields the FRF's

$$H_1(\omega) = K_d^{(1)} + iK_m\omega \tag{65}$$

$$H_3(\omega_1,\omega_2,\omega_3) = \frac{1}{6}K_d^{(3)} \tag{66}$$

The magnitude and phase of a typical Morison equation H_1 are given in Figure 8. The linear dynamics of Morison's equation are a little strange in that $|H_1(\omega)| \longrightarrow \infty$ as $\omega \longrightarrow \infty$ also the phase angle tends to $\frac{\pi}{2}$ as $\omega \longrightarrow \infty$. This means that a high frequency wave - however small in amplitude - incident on the cylinder can generate a very high force which leads the wave by a quarter of a cycle.

The second order FRF vanishes as a consequence of the fact that nonlinearity is an odd power. This is not due to the approximation procedure; $u|u|$ is an odd function so any least-squares polynomial approximation will also be odd. Because of this, Morison's equation cannot generate a low-frequency drift component under harmonic excitation i.e. in regular waves. Such effects are produced by difference combinations of frequencies which are generated by the even order FRF's. The situation is different if a current is present. In a steady current of velocity u_0 and wave-induced velocity $u(t)$, the drag term becomes proportional to $(u+u_0)|(u+u_0)|$ which is then approximated by $\alpha_1(u+u_0)+\alpha_3(u+u_0)^3$ say. This expression has a u^2 term which will generate a constant but non-vanishing H_2 function. The use of quadratic transfer functions to model low frequency forces is well established in the literature of fluid-loading, see for example [17].

The third order FRF for the approximate Morison system is simply a constant, all components in the third order output $y_3(t)$ appear with the same amplitude independently of input frequencies; therefore there are no third order 'resonances'.

Having obtained the higher order FRF's, one can substitute into equations (12) and (14) and thence into (11) to obtain the nonlinear spectral representation of the force in terms of the velocity spectrum $U(\omega)$

$$F(\omega) = (K_d^{(1)} + iK_m\omega)U(\omega) +$$

$$\frac{K_d^{(3)}}{24\pi^2}\int_{-\infty}^{+\infty}\int_{-\infty}^{+\infty} d\omega_1 d\omega_2 U(\omega_1)U(\omega_2)U(\omega-\omega_1-\omega_2) \tag{67}$$

Because H_3 is a constant, it can be taken out of the integral for the third order component of the output as above. The resulting integral can then be written as a convolution product.

$$U*U*U(\omega) = \int_{-\infty}^{+\infty}\int_{-\infty}^{+\infty} d\omega_1 d\omega_2 U(\omega_1)U(\omega_2)U(\omega-\omega_1-\omega_2)$$

This allows the following compact form for the force spectrum

$$F(\omega) = (K_d^{(1)} + iK_m\omega)U(\omega) + \frac{K_d^{(3)}}{24\pi^2}U*U*U(\omega) \tag{68}$$

This type of equation was introduced in [18], it appears to have been initially obtained by Bendat and Piersol for Shell International Petroleum. The derivation was by direct Fourier transformation of the cubic approximation to Morison's equation. A study of the efficacy of this equation based on experimental data obtained in the De Voorst wave flume is presented in [19].

It is only a little more difficult to determine the higher order FRFs for the Duffing-Morison equation,

$$\alpha_1\ddot{F} + \alpha_2\dot{F} + F + \alpha_3 F|F| = \frac{1}{2}\rho D C_d u|u| + \frac{1}{4}\pi\rho D^2 C_m \dot{u} \tag{69}$$

which was examined in [3] as a possible extension to Morison's equation. On approximating the $u|u|$ and $F|F|$ terms by cubics and relabelling, one obtains

$$\alpha_1\ddot{F} + \alpha_2\dot{F} + \gamma_1 F + \gamma_3 F^3 = K_d^{(1)}u + K_d^{(3)}u^3 + K_m\dot{u} \tag{70}$$

where γ_1, γ_3, $K_d^{(1)}$ and $K_d^{(3)}$ are now functions of the approximating intervals. Harmonic probing of this system yields the higher order FRF's

$$H_1(\omega) = \frac{iK_m\omega + K_d^{(1)}}{-\alpha_1\omega^2 + i\alpha_2\omega + \gamma_1} \tag{71}$$

$$H_2(\omega_1,\omega_2,\omega_3) = \frac{1}{6}\frac{K_d^{(3)} - \gamma_3 H_1(\omega_1)H_1(\omega_2)H_1(\omega_3)}{-\alpha_1(\omega_1+\omega_2+\omega_3)^2 + i\alpha_2(\omega_1+\omega_2+\omega_3)} \tag{72}$$

Note that $H_1(\omega) \longrightarrow 0$ as $\omega \longrightarrow \infty$ showing that the Morison-Duffing equation does not suffer from the high frequency 'instability' which is present for Morison's equation. This is prevented by the addition of the $\ddot{F}$ and $\dot{F}$ terms. Further, the equation has much more complex third order dynamics. The poles in equation (72) will produce a maximum in the third order output when the combination resonance condition $\omega_1 + \omega_2 + \omega_3 = \omega_r$ is met where ω_r is the linear resonant frequency given by $\omega_r = \sqrt{\frac{\gamma_1}{\alpha_1}}$

6 Higher Order FRF's from Experimental Data.

In the first part of this study [1], NARMAX models were fitted to measured flow velocity and force data for a variety of different flows. The higher order FRF's corresponding to these models are presented below.

The first set of data were obtained from U-tube experiments by Obasaju *et.al.* [4]. A horizontal cylinder was placed in a planar oscillatory flow, so the excitation $u(t)$ is harmonic. The data is described in more detail in [1]. Results were obtained for KC values of 3.31, 6.48. 11.88, 17.5 and 34.68. The Stokes parameter $\beta = Re/KC$, where Re is the Reynolds number, was held constant at a value of 417. The data for KC of 3.31 and 6.48 were essentially linear, inertia-dominated and Morison's equation proved adequate for prediction purposes. For this reason the NARMAX study was restricted to the data for the higher values of KC. The following models were obtained: for $KC = 11.88$,

$$\begin{aligned} F_i &= 0.18021\times 10F_{i-1} - 0.78516F_{i-2} \\ &- 0.41016\times 10^{-1}F_{i-4} - 0.41113u_{i-3}u_{i-3}u_{i-3} \\ &+ 0.92188u_iu_iu_i - 0.31250F_{i-1}u_iu_i \\ &+ 0.42653\times 10^4F_{i-4}u_{i-3} + 0.84966\times 10^4F_{i-4}u_i \\ &+ 0.33159\times 10^{-1}F_{i-1}F_{i-2}u_i - 0.12659\times 10^5F_{i-4}u_{i-1} \end{aligned} \tag{73}$$

for KC =17.5,

$$\begin{aligned} F_i &= 0.16842\times 10F_{i-1} - 0.64108F_{i-2} \\ &- 0.26385\times 10^{-1}F_{i-1}F_{i-1}F_{i-1} - 0.80901\times 10^{-1}u_i \\ &- 0.94940\times 10^{-1}u_{i-2} + 0.83598u_iu_iu_i \\ &- 0.58117F_{i-3}u_{i-3}u_{i-3} + 0.14757F_{i-2}F_{i-4}u_{i-3} \end{aligned} \tag{74}$$

and for $KC = 34.68$,

$$\begin{aligned} F_i &= 0.16968 \times 10F_{i-1} && - 0.92220F_{i-2} \\ &+ 0.62466 \times 10^{-1}F_{i-1}F_{i-1}F_{i-1} && - 0.58983u_{i-3}u_{i-3}u_{i-3} \\ &+ 0.15208 \times 10u_iu_iu_i && - 0.80145F_{i-1}u_iu_i \\ &+ 0.46783 \times 10^{-2}F_{i-4}F_{i-4} && + 0.22397F_{i-3} \\ &- 0.33093 \times 10^{-1}u_{i-3} \end{aligned} \tag{75}$$

In each of these cases, the NARMAX model gave a very substantial improvement over Morison in predicting the force. However, each model contains different terms, particularly the third order products. Following the argument of section 4, one might expect a greater degree of consistency in the frequency domain. Recalling that Morison's equation predicts a vanishing H_2 and constant H_3, one can determine the higher order FRF's for the models above to see if there is any deviation from this. Regarding the linear behaviour of the models, in all cases the H_1 functions showed a peak value on or near $f = 0$, the variation thereafter with frequency being monotonic decrease. This is in contradiction with the result expected from Morison's equation (Figure 8) in which the H_1 gain *increases* monotonically with frequency. The actual observed results are therefore more in keeping with what would be expected on the grounds of stability. In all these cases, the H_2 functions either vanished or had very small magnitude and were devoid of any interesting structure.

The $H_3(\omega_1, \omega_2, \omega_1)$ functions from the NARMAX models are shown in Figures 9 to 11. The frequency limit for the plot in each case is the normalised Nyquist frequency of 0.5. In each case the magnitude and phase surfaces are given together with the corresponding contour maps. Note that the region of validity of the surfaces - the higher order generalisation of the Nyquist interval is larger if H_2 vanishes, the Nyquist region in this case is indicated by the solid lines in Figure 9d.

The first of the figures is for the $KC = 11.88$ data which was sampled at 71 points per cycle. The dominant feature is the significant ridge along the line joining A and B in Figure 9c; this is over the line $2f_1 + f_2 = 0$, and is a combination resonance due to the peak in $H_1(f_1)$ at $f_1 = 0$ If the excitation frequencies satisfy this condition, the output will be at the frequency $f_1 + f_2 + f_3 = f_1 - 2f_1 + f_1 = 0$; this represents a transfer of energy to the d.c. component of the output. This effect would not be observed in a U-tube experiment where a single excitation frequency is necessary. Another feature of interest is the valley between the points C and D along the line $2f_1 + f_2 = f_v$, where f_v is a little less than the Nyquist frequency; if the excitation frequencies combine to give a point on this line there will be no significant nonlinear effects. Given in Figure 10 is H_3 for the $KC = 17.5$ data, sampled at 112 points per cycle. This has exactly the same features as the previous H_3; note that the peak values of the magnitude surfaces are also very similar i.e. 26.5 db and 26.1 db. Figure 11 shows H_3 from the $KC = 34.68$ data sampled at 71 points per cycle, the same features are present again, the only difference in this case is that the peak gain is up to 118 db, indicating very significant nonlinear effects if the condition $2f_1 + f_2$ is met. In conclusion for the U-tube data, the H_3 functions are not constant as for the Morison equation, in fact they show pronounced ridges. Further, there is good agreement in the positions of these features between the H_3's for the different KC values. Note that there is a common structure for both the gain surfaces and the phase surfaces.

The second set of experimental data examined in [1] was obtained from a test at the De Voorst wave flume facility. The experiment is described in more detail in [1] and [20]. The cylinder was placed in irregular waves with a JONSWAP spectrum

with peak frequency 0.2 Hz; the excitation was quite narrow-banded. The sampling frequency adopted was 20 Hz. In general, the force data from the particular test examined (run OA1F1) was linear inertia-dominated and Morison's equation proved perfectly adequate for prediction purposes. As the magnitude of the transverse force is an indicator of vortex shedding, a NARMAX model was fitted to 1000 point samples of in-line force and velocity around the point at which the transverse force force on the cylinder was a maximum. The result was,

$$\begin{aligned} F_i &= 0.10527 \times 10 F_{i-1} - 0.24170 F_{i-4} \\ &- 0.19254 \times 10^3 u_{i-4} + 0.18877 \times 10^3 u_i \\ &+ 0.19028 \times 10^2 u_{i-4} u_{i-4} u_{i-4} + 0.83766 \times 10^{-2} F_{i-1} F_{i-1} u_{i-4} \\ &- 0.77932 \times 10^{-2} F_{i-1} F_{i-2} u_{i-3} \end{aligned} \tag{76}$$

H_1 for this system is shown in Figure 12. It is interesting that the presence of a linear resonance (at $f = f_{res}$) is indicated, the peak shown is not at the main forcing frequency which is at 0.01 normalised. After the peak H_1 decreases overall. H_3 for the system is shown in Figure 13; similar ridges to those which characterised the U-tube data are present. A double peaked ridge along the line CD shows peaks along $2f_1 + f_2 = \pm f_{res}$ where f_{res} is the linear resonant frequency; this shows that there will be a transfer of energy to the linear resonance. This feature is not as sharply indicated as for the U-tube data, this can probably be attributed to the smallness of the nonlinear component of the force data, which makes accurate identification difficult. The dominant feature in the H_3 appears to be a ridge along the line ADC corresponding to $f_1 = f_3 = 0$. A NARMAX model was also fitted to data centred on the same point in the record but decimated by a factor of 2. This gives an effective sampling frequency of 10 Hz. The model obtained was

$$\begin{aligned} F_i &= 0.85124 F_{i-1} - 0.29028 F_{i-3} \\ &- 0.25433 \times 10^2 u_{i-4} + 0.73679 \times 10^3 u_i \\ &- 0.71581 \times 10^3 u_{i-1} + 0.47754 \times 10^2 u_{i-4} u_{i-4} u_{i-4} \\ &+ 0.10364 \times 10^{-2} F_{i-1} F_{i-1} u_{i-4} \end{aligned} \tag{77}$$

H_1 is given in Figure 14. Again, one observes a peak. This occurs at twice the normalised frequency as previously, i.e. at the same absolute frequency f_{res} given that the sampling frequency has halved. This supports the conclusion that the linear 'resonance' is a feature of the system. This is not predicted by Morison's equation. H_3 is shown in Figure 15. As before, characteristic ridges are present along $2f_1 + f_2 = \pm f_{res}$ (lines AB and CD in Figure 15c), although not very sharply defined. The features are clearest in the contour map for the magnitude $|H_3|$ (Figure 15c). Unusually, the ridge at $f_1 = 0$ which dominated Figure 13c is absent, this may be due to the fact the the nonlinear component of the data was decreased by the decimation procedure making identification of nonlinear terms even more difficult.

The final sample of data considered in [1] was recorded from the Christchurch Bay Tower [21]. In this case the cylinder was in a random directional sea with current. As in the wave flume experiments the wave spectrum was very sharply peaked, in this case at approximately 0.1 Hz; the sampling frequency was 10 Hz. In order to minimise the effects of directionality, a NARMAX model was fitted to the 1000 point data segment which had the minimum RMS velocity transverse to the predominant wave direction. The data was decimated by a factor of 2, giving an effective sampling frequency of 5 Hz. The resulting model was,

$$
\begin{aligned}
F_i = {} & 0.18615 \times 10 F_{i-1} && - 0.11551 \times 10 F_{i-2} \\
& - 0.66218 \times 10^{-5} F_{i-1} F_{i-1} F_{i-1} && - 0.36266 \times 10^{-6} F_{i-1} F_{i-1} F_{i-4} \\
& - 0.21047 F_{i-1} u_{i-4} u_{i-4} && + 0.19212 F_{i-4} u_i u_i \\
& - 0.42832 F_{i-3} u_i u_{i-4} && + 0.42050 F_{i-2} u_{i-3} u_{i-3} \\
& - 0.20219 \times 10^{-3} F_{i-3} F_{i-3} && + 0.14279 \times 10^{-3} F_{i-2} F_{i-5} \\
& - 0.79306 \times 10^{-3} F_{i-1} F_{i-2} u_i && + 0.48154 \times 10^{-3} F_{i-1} F_{i-1} u_{i-4} \\
& + 0.50511 \times 10^{2} u_{i-3} u_{i-4} u_{i-4} && + 0.18365 \times 10^{3} u_i u_{i-4} u_{i-4} \\
& - 0.22708 \times 10^{3} u_{i-1} u_{i-4} u_{i-4} && + 0.13557 \times 10^{-4} F_{i-2} F_{i-2} F_{i-2} \\
& - 0.32915 \times 10^{-4} F_{i-1} F_{i-2} F_{i-2} && + 0.24301 \times 10^{-5} F_{i-1} F_{i-1} F_{i-3} \\
& + 0.24703 \times 10^{-4} F_{i-1} F_{i-1} F_{i-2} && - 0.36463 F_{i-5} \\
& + 0.14370 F_{i-4} && + 0.14133 F_{i-6} \\
& + 0.11428 \times 10^{3} u_i && - 0.24760 \times 10^{3} u_{i-1} \\
& + 0.20084 \times 10^{3} u_{i-2} && + 0.28620 F_{i-3} \\
& - 0.44304 \times 10^{2} u_{i-3} && + 0.27294 \times 10^{2} u_{i-5} \\
& - 0.46985 \times 10^{2} u_{i-4}
\end{aligned}
\tag{78}
$$

Harmonic probing of this model yielded the H_1 function given in Figure 16, which has a prominent peak at a frequency quite distinct from the forcing frequency ($\approx$ 0.005 normalised = 0.24 Hz). The H_2 function is shown in Figure 17, its features are not very sharply defined, probably due to the fact that the component of the current in the predominant wave direction was small; this makes identification of the second order component of the force difficult. It is clearest from the contour map of the gain surface (Figure 17c) that there are ridges at $f_1 + f_2 = \pm f_{res}$ (along lines AB and CD). Note that the peak gain (Figure 17a) is 46 db compared with 51 db for H_1, this shows that significant second order nonlinear effects can be expected under certain excitations. Finally, the H_3 surface is given in Figure 18 and shows a marked occurrence of the ridges at $2f_1 + f_2 = f_{res}$ (lines AB and CD in Figure 18c) which have been observed in the other cases. Note that the peak gain (Figure 18a) is 81 db, very large compared to H_2 and H_1.

All the results described above show remarkable consistency; however, they must be interpreted with great care. The reason for this is quite simple. In order to obtain unambiguous results from *any* system identification procedure, the input function, in this case $u(t)$, used to force the system must excite all modes of interest; effectively, the system should be forced over as broad a range of frequencies as possible. Previously, most experiments in the field of wave loading have concentrated on simulating specific conditions. However, for the purposes of obtaining information about wave loading mechanisms from system identification procedures it would be useful to carry out an experiment using broadband random excitation.

7 Conclusions.

It appears from the results obtained here, that some systematic structure is present in higher order FRF's which is not predicted by Morison's equation. This structure is common to wave loading data from several quite different flows. It is obtained from the frequency domain analysis of NARMAX models which have quite different structures. The implication is that some of the variation in the NARMAX models is due to the lack of uniqueness of a discrete time description for a system, i.e. it is not completely due to differences in the underlying physics of the flows. It follows that there may be an extension to Morison's equation valid in all flows which

will reproduce the high frequency components of wave loading data better than the Morison equation. Recent results by Billings and co-workers at the University of Sheffield suggest that it is possible to obtain a continuous-time representation of a system from the higher order FRF's. Research is in progress to determine if the H_n functions described in this paper can furnish such a representation for the wave loading case.

Acknowledgements.

Thanks are due to Delft Hydraulics for access to the wave force data obtained in the Delta flume in their De Voorst facility. This data was provided with the assistance of Malcolm Birkinshaw of the Health and Safety Executive and Professor Peter Bearman and Martin Davies of Imperial college. In particular, the help provided by Martin Davies in translating data into a useful format is much appreciated. Thanks are also due to Dr. Emmanuel Obasaju for making available unpublished data from his experimental work undertaken as a research associate at Imperial College. This project is supported by the Offshore Safety Division of the Health and Safety Executive through the Marine Technology Directorate's managed programme on the Behaviour of Fixed and Compliant Offshore Structures. This paper will comprise part of the final report to the Health and Safety Executive (to be published by HMSO).

References

[1] Worden (K.), Billings (S.A.), Stansby (P.K.) & Tomlinson (G.R.) 1991 *Submitted to Journal of Fluids and Structures.* Identification of nonlinear wave loading forces. Part I. Time-domain analysis.

[2] Morison (J.R.), O'Brien (M.P.), Johnson (J.W.) & Schaf (S.A.) 1950 *Petroleum Transactions* **189** pp.149-157. The force exerted by surface waves on piles.

[3] Stansby (P.K.), Worden (K.), Billings (S.A.) & Tomlinson (G.R.) 1991 *To appear in Applied Ocean Research.* Improved wave force classification using system identification.

[4] Obasaju (E.D.), Bearman (P.W.) & Graham (J.M.R.) 1988 *Journal of Fluid Mechanics* **196** pp.467-494. A study of forces, circulation and vortex patterns around a circular cylinder in oscillating flow.

[5] Schetzen (M.) 1980 *The Volterra and Wiener Theories of Nonlinear Systems.* John Wiley Interscience Publication. New York.

[6] Billings (S.A.) & Tsang (K.M.) 1989 *Mechanical Systems and Signal Processing* **3** pp.341-359. Spectral analysis for nonlinear systems, part II: Interpretation of nonlinear frequency response functions.

[7] Volterra (V.) 1959 *Theory of Functionals and Integral equations.* Dover Publications, New York.

[8] Barrett (J.F.) 1963 *Journal of Electronics and Control* **15** pp.567-615. The use of functionals in the analysis of nonlinear systems.

[9] Gifford (S.J.) 1990 *Journal of Sound and Vibration* **135** pp.289-317. Recent advances in the application of functional series to non-linear structures.

[10] Storer (D.M.) 1991 *Dynamic Analysis of Nonlinear Structures Using Higher Order Frequency Response Functions.* Ph.D. Thesis, Department of Engineering, University of Manchester.

[11] Bedrossan (E.) & Rice (S.O.) 1971 *Proceedings IEEE* **59** pp.1688-1707. The output properties of Volterra systems driven by harmonic and Gaussian inputs.

[12] Peyton Jones (J.C.) & Billings (S.A.) 1989 *International Journal of Control* **50** pp.1925-1940. Recursive algorithm for computing the frequency response of a class of non-linear difference equation models.

[13] Leontaritis (I.J.) & Billings (S.A.) 1985 *International Journal of Control* **41** pp.303-328. Input-output parametric models for nonlinear systems. Part I: deterministic nonlinear systems.

[14] Leontaritis (I.J.) & Billings (S.A.) 1985 *International Journal of Control* **41** pp.329-344. Input-output parametric models for nonlinear systems. Part II: stochastic nonlinear systems.

[15] Billings (S.A.) & Tsang (K.M.) 1989 *Mechanical Systems and Signal Processing* **3** pp.319-339. Spectral analysis for nonlinear systems, part I: Parametric nonlinear spectral analysis.

[16] Palm (G.) & Poggio (T.) 1977 *SIAM Journal on Applied Mathematics* **33** part 2. The Volterra representation and the Wiener expansion: validity and pitfalls.

[17] Eatock Taylor (R.) 1990 in *Environmental Forces on Offshore Structures and Their Prediction. Kluwer Academic Press.* pp.323-349. Predictions of loads on floating production systems.

[18] Vugts (J.H.) & Bouquet (A.G.) 1985 *Proceedings of BOSS 1985 - Delft* pp239-253. A non-linear frequency domain description of wave forces on an element of a vertical pile in random seas.

[19] Bliek (A.) & Klopman (G.) 1988 *proceedings of BOSS 1988* pp.821-840. Non-linear frequency modelling of wave forces on large vertical and horizontal cylinders in random waves.

[20] Davies (M.J.S.), Graham (J.M.R.), & Bearman (P.W.) 1990 in *Environmental Forces on Offshore Structures and Their Prediction. Kluwer Academic Press.* pp.113-136. In-line forces on fixed cylinders in regular and random waves.

[21] Bishop (J.R.) 1979 *National Maritime Institute report no. NMI R57* Aspects of large scale wave force experiments and some early results from Christchurch Bay.

Appendix A. Frequency Domain Representation of the Volterra Series.

Although the calculation which leads from equation (5) to equation (11) in the main body of the paper is fairly well-known, it is included here in order that the presentation be reasonably self-contained.

The calculation is simplified by adopting a useful integral representation of the Dirac delta function. One begins with Fourier's theorem for the Fourier transform.

$$f(t) = \frac{1}{2\pi}\int_{-\infty}^{+\infty} d\omega e^{i\omega t}\left\{\int_{-\infty}^{+\infty} d\tau e^{-i\omega\tau} f(\tau)\right\} \tag{79}$$

which gives

$$f(0) = \frac{1}{2\pi}\int_{-\infty}^{+\infty} d\omega\left\{\int_{-\infty}^{+\infty} d\tau e^{-i\omega\tau} f(\tau)\right\} = \int_{-\infty}^{+\infty} d\tau\left\{\frac{1}{2\pi}\int_{-\infty}^{+\infty} d\omega e^{-i\omega\tau}\right\} f(\tau) \tag{80}$$

Now, the defining property of the Dirac delta $\delta(\tau)$ is the projection property (which is used frequently thoroughout this study)

$$f(a) = \int_{-\infty}^{+\infty} d\tau\delta(\tau - a) f(\tau) \tag{81}$$

which implies,

$$f(0) = \int_{-\infty}^{+\infty} d\tau\delta(\tau) f(\tau)$$

So, (80) allows one to make the identification

$$\delta(\tau) = \frac{1}{2\pi}\int_{-\infty}^{+\infty} d\omega e^{-i\omega\tau} = \frac{1}{2\pi}\int_{-\infty}^{+\infty} d\omega e^{i\omega\tau} \tag{82}$$

Thus, the delta function can be used in the sequel simply as a means of encoding Fourier's inversion theorem in the calculation. It is assumed throughout that interchange of the order of integration in repeated integrals is valid.

The calculation of $Y_1(\omega)$ in equation (11) is elementary. Equation (6) yields

$$Y_1(\omega) = \mathcal{F}[y_1(t)] = \int_{-\infty}^{+\infty} dt e^{-i\omega t}\int_{-\infty}^{+\infty} d\tau h_1(\tau) x(t-\tau)$$

$$= \int_{-\infty}^{+\infty} dt\int_{-\infty}^{+\infty} d\tau e^{-i\omega t} h_1(\tau)\left\{\frac{1}{2\pi}\int_{-\infty}^{+\infty} d\Omega e^{i\Omega(t-\tau)} X(\Omega)\right\}$$

Rearranging and changing the order of integration gives

$$= \int_{-\infty}^{+\infty} d\Omega\left\{\int_{-\infty}^{+\infty} d\tau e^{-i\omega\tau} h_1(\tau)\right\} X(\Omega)\left\{\frac{1}{2\pi}\int_{-\infty}^{+\infty} dt e^{it(\omega-\Omega)}\right\}$$

$$= \int_{-\infty}^{+\infty} d\Omega H_1(\omega) X(\Omega)\delta(\omega - \Omega) = H_1(\omega)\int_{-\infty}^{+\infty} d\Omega X(\Omega)\delta(\omega - \Omega) = H_1(\omega) X(\omega)$$

as required. The calculation for $Y_2(\omega)$ proceeds in exactly the same fashion:

$$Y_2(\omega) = \mathcal{F}[y_2(t)] = \int_{-\infty}^{+\infty} dt e^{-i\omega t} \int_{-\infty}^{+\infty} \int_{-\infty}^{+\infty} d\tau_1 d\tau_2 h_2(\tau_1, \tau_2) x(t-\tau_1) x(t-\tau_2)$$

$$= \int_{-\infty}^{+\infty} \int_{-\infty}^{+\infty} \int_{-\infty}^{+\infty} dt d\tau_1 d\tau_2 e^{-i\omega t} h_2(\tau_1, \tau_2) \cdot$$

$$\left\{ \frac{1}{2\pi} \int_{-\infty}^{+\infty} d\omega_1 e^{i\omega_1(t-\tau_1)} X(\omega_1) \right\} \left\{ \frac{1}{2\pi} \int_{-\infty}^{+\infty} d\omega_2 e^{i\omega_2(t-\tau_2)} X(\omega_2) \right\}$$

Rearranging and interchanging order gives

$$Y_2(\omega) = \frac{1}{(2\pi)} \int_{-\infty}^{+\infty} \int_{-\infty}^{+\infty} d\omega_1 d\omega_2 \left\{ \int_{-\infty}^{+\infty} \int_{-\infty}^{+\infty} d\tau_1 d\tau_2 h_2(\tau_1, \tau_2) e^{-i(\omega_1 \tau_1 + \omega_2 \tau_2)} \right\} \cdot$$

$$\left\{ \frac{1}{(2\pi)} \int_{-\infty}^{+\infty} dt e^{-it(\omega - \omega_1 - \omega_2)} \right\} X(\omega_1) X(\omega_2)$$

Applying the definition of $H_2(\omega_1, \omega_2)$ from (11), and using the representation of the delta function above, yields

$$Y_2(\omega) = \frac{1}{(2\pi)} \int_{-\infty}^{+\infty} \int_{-\infty}^{+\infty} d\omega_1 d\omega_2 H_2(\omega_1, \omega_2) X(\omega_1) X(\omega_2) \delta(\omega - \omega_1 - \omega_2)$$

A final integration over ω_2 gives

$$Y_2(\omega) = \frac{1}{(2\pi)} \int_{-\infty}^{+\infty} d\omega_1 H_2(\omega_1, \omega - \omega_1) X(\omega_1) X(\omega - \omega_1)$$

which is equation (13) as required. The evaluation of $H_3(\omega)$ proceeds exactly as above. The above calculations can of course be carried out without using δ functions. The alternative, more rigorous, approach is to use convolution products.

Figure Captions.

Figure 1. Comparison between simulated Duffing oscillator data and prediction by NARMAX model.

Figure 2. $H_1(f)$ for Duffing oscillator system: (a) exact magnitude, (b) exact phase, (c) NARMAX model magnitude, (d) NARMAX model phase.

Figure 3. $H_2(f_1, f_2)$ for Duffing oscillator system: (a) exact magnitude, (b) exact phase, (c) NARMAX model magnitude, (d) NARMAX model phase.

Figure 4. Contour maps of $H_2(f_1, f_2)$ for Duffing oscillator system: (a) exact magnitude, (b) exact phase, (c) NARMAX model magnitude, (d) NARMAX model phase.

Figure 5. $H_3(f_1, f_2, f_1)$ for Duffing oscillator system: (a) exact magnitude, (b) exact phase, (c) NARMAX model magnitude, (d) NARMAX model phase.

Figure 6. Contour maps of $H_3(f_1, f_2, f_1)$ for Duffing oscillator system: (a) exact magnitude, (b) exact phase, (c) NARMAX model magnitude, (d) NARMAX model phase.

Figure 7. H_1, H_2 and H_3 components in the Duffing system output for excitation by a unit sinusoid: (a) exact magnitude, (b) exact phase, (c) NARMAX model magnitude, (d) NARMAX model phase.

Figure 8. $H_1(f)$ magnitude and phase for Morison equation.

Figure 9. $H_3(f_1, f_2, f_1)$ from NARMAX fit to U-tube data with KC of 11.88. (a) Magnitude, (b) phase, (c) magnitude contour map, (d) phase contour map.

Figure 10. $H_3(f_1, f_2, f_1)$ from NARMAX fit to U-tube data with KC of 17.5. (a) Magnitude, (b) phase, (c) magnitude contour map, (d) phase contour map.

Figure 11. $H_3(f_1, f_2, f_1)$ from NARMAX fit to U-tube data with KC of 34.68. (a) Magnitude, (b) phase, (c) magnitude contour map, (d) phase contour map.

Figure 12. $H_1(f)$ from NARMAX fit to De Voorst data sampled at 20Hz. (a) Magnitude, (b) phase.

Figure 13. $H_3(f_1, f_2, f_1)$ from NARMAX fit to De Voorst data sampled at 20Hz. (a) Magnitude, (b) phase, (c) magnitude contour map, (d) phase contour map.

Figure 14. $H_1(f)$ from NARMAX fit to De Voorst data sampled at 10Hz. (a) Magnitude, (b) phase.

Figure 15. $H_3(f_1, f_2, f_1)$ from NARMAX fit to De Voorst data sampled at 10Hz. (a) Magnitude, (b) phase, (c) magnitude contour map, (d) phase contour map.

Figure 16. $H_1(f)$ from NARMAX fit to Christchurch Bay data. (a) Magnitude, (b) phase.

Figure 17. $H_2(f_1, f_2)$ from NARMAX fit to Christchurch Bay data. (a) Magnitude, (b) phase, (c) magnitude contour map, (d) phase contour map.

Figure 18. $H_3(f_1, f_2, f_1)$ from NARMAX fit to Christchurch Bay data. (a) Magnitude, (b) phase, (c) magnitude contour map, (d) phase contour map.

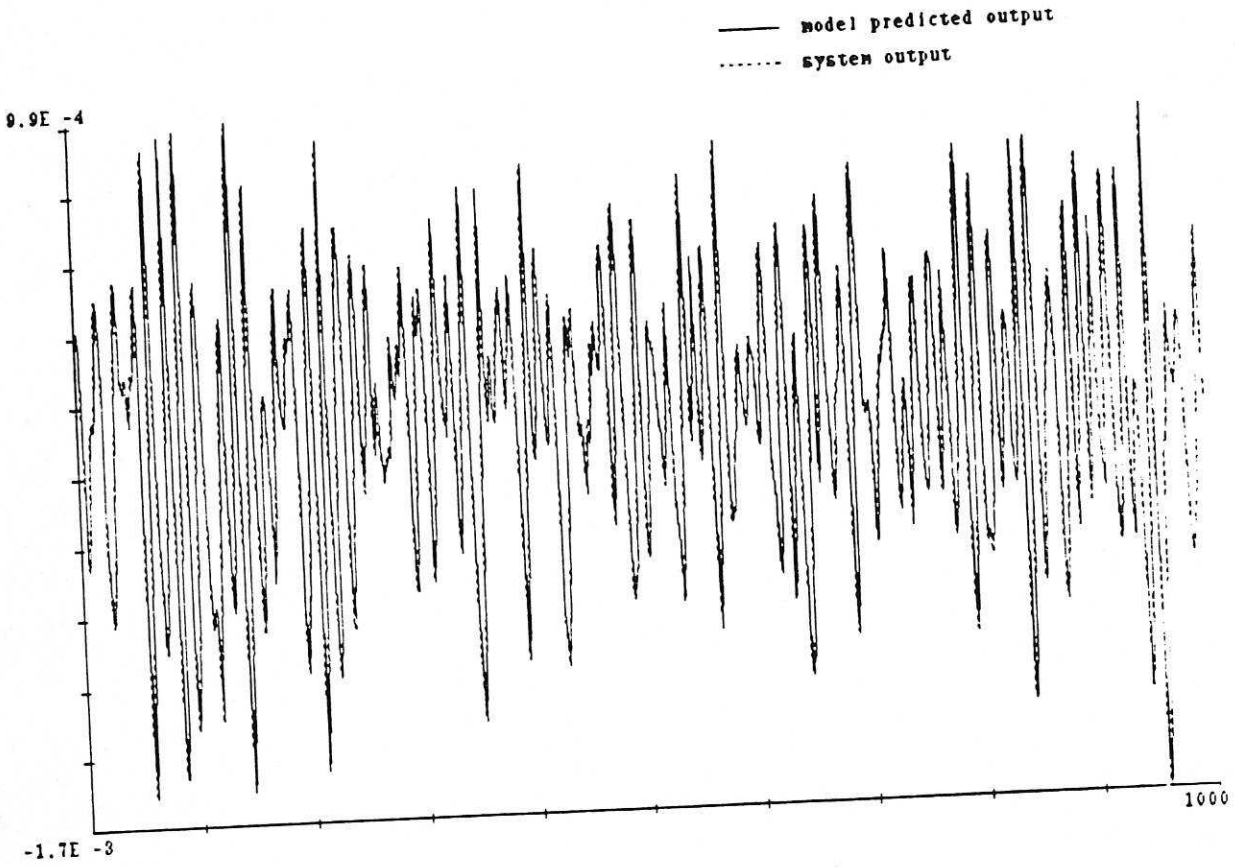
model predicted output
system output
9.9E -4
-1.7E -3
1000

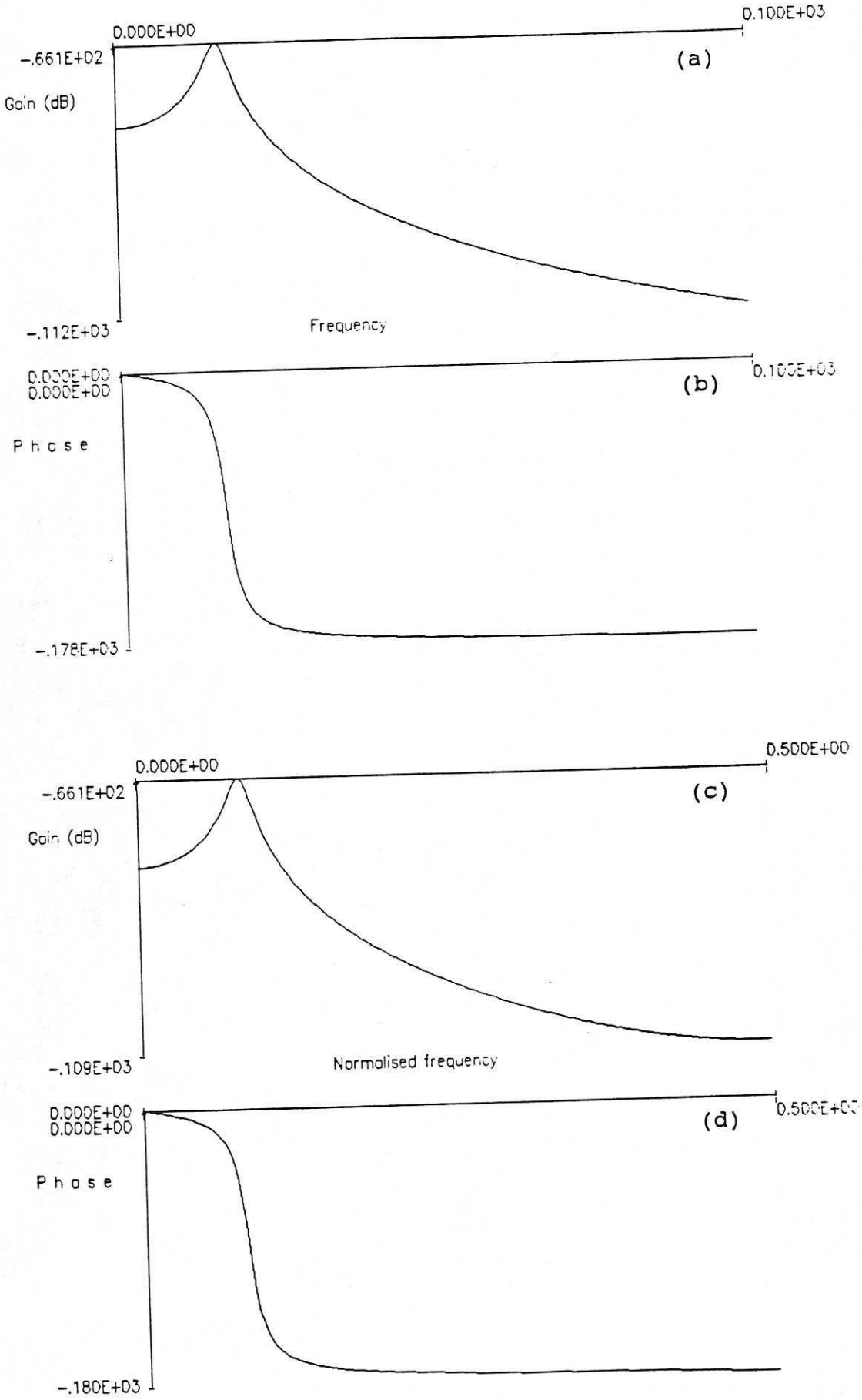
0.000E+00
0.100E+03
-.661E+02
(a)
Gain (dB)
-.112E+03
Frequency
0.000E+00
0.000E+00
0.100E+03
(b)
Phase
-.178E+03
0.000E+00
0.500E+00
-.661E+02
(c)
Gain (dB)
-.109E+03
Normalised frequency
0.000E+00
0.000E+00
0.500E+00
(d)
Phase
-.180E+03

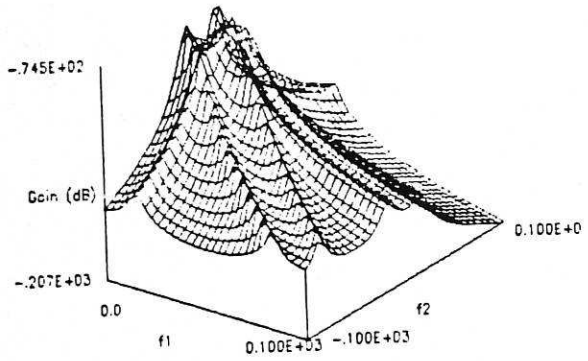
-.745E+02
Gain (dB)
-.207E+03
0.0
f1
0.100E+03
-.100E+03
f2
0.100E+0

(a)

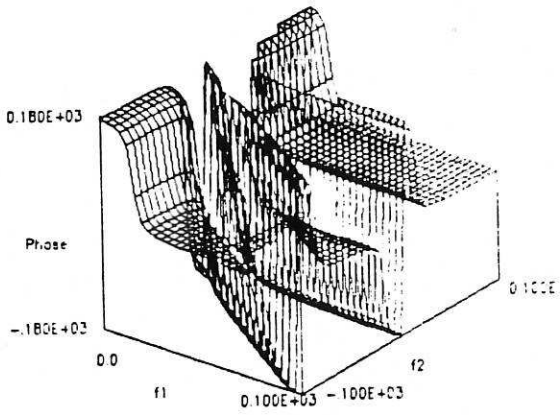
0.180E+03
Phase
-.180E+03
0.0
f1
0.100E+03
-.100E+03
f2

(b)

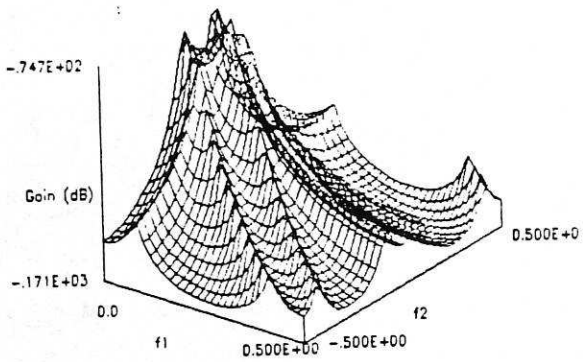
-.747E+02
Gain (dB)
-.171E+03
0.0
f1
0.500E+00
-.500E+00
f2
0.500E+0

(c)

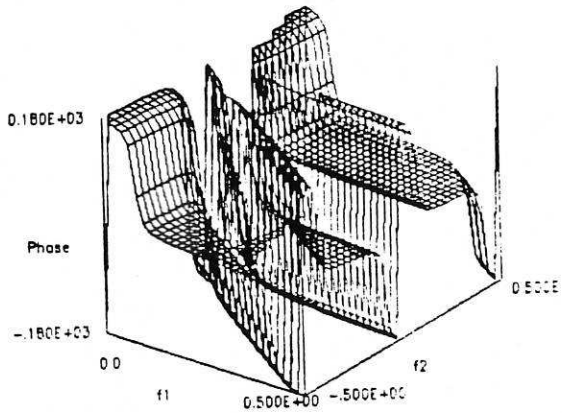
0.180E+03
Phase
-.180E+03
0.0
f1
0.500E+00
-.500E+00
f2

(d)

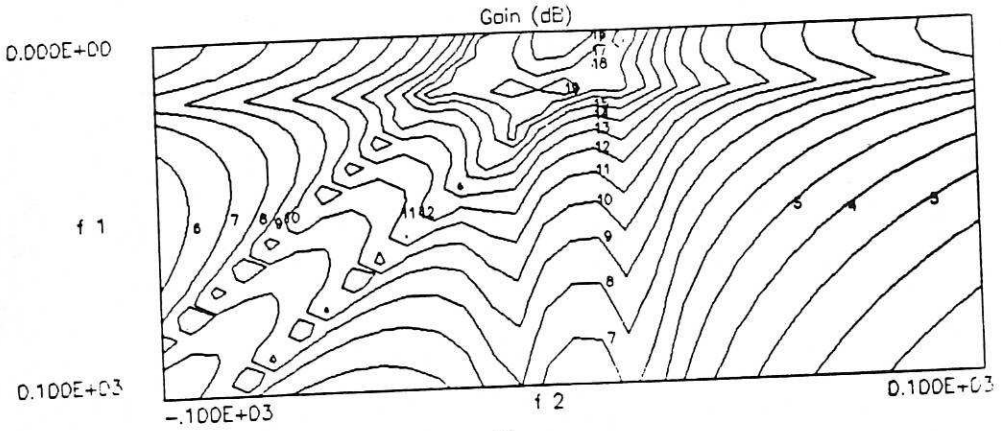
Gain (dB)
0.000E+00
f 1
0.100E+03
-.100E+03
f 2
0.100E+03

(a)

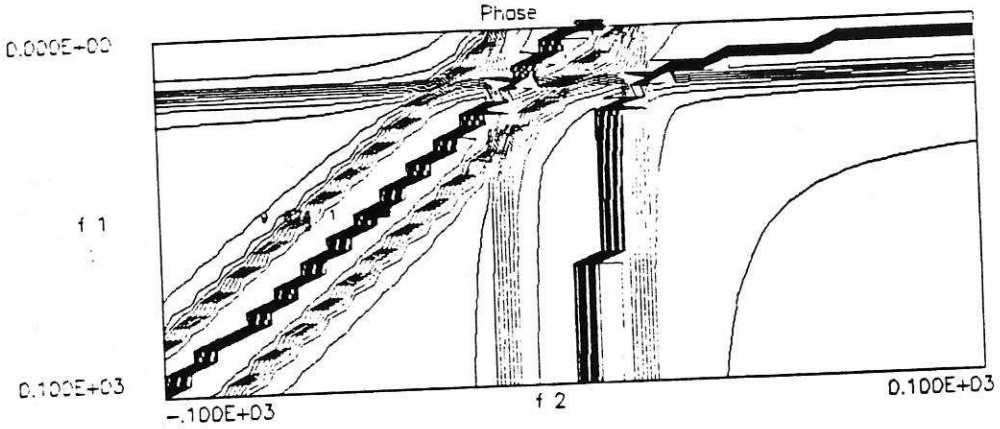
Phase
0.000E+00
f 1
0.100E+03
-.100E+03
f 2
0.100E+03

(b)

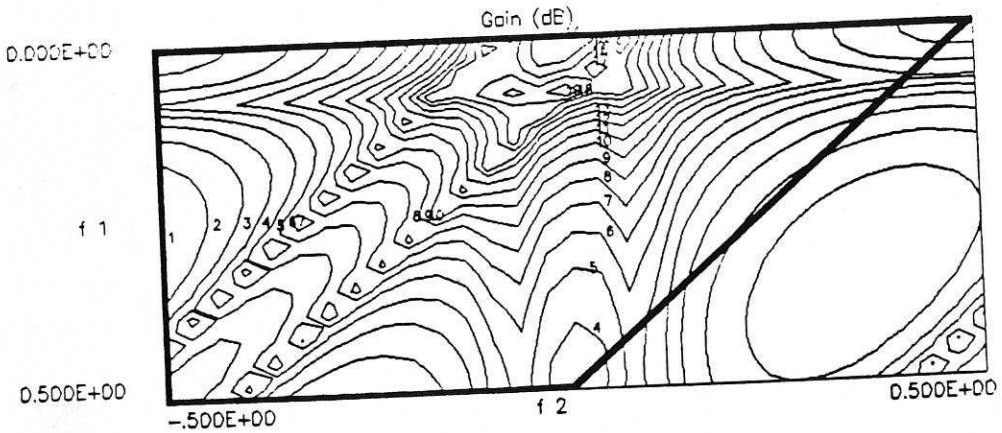
Gain (dB)
0.000E+00
f 1
0.500E+00
-.500E+00
f 2
0.500E+00

(c)

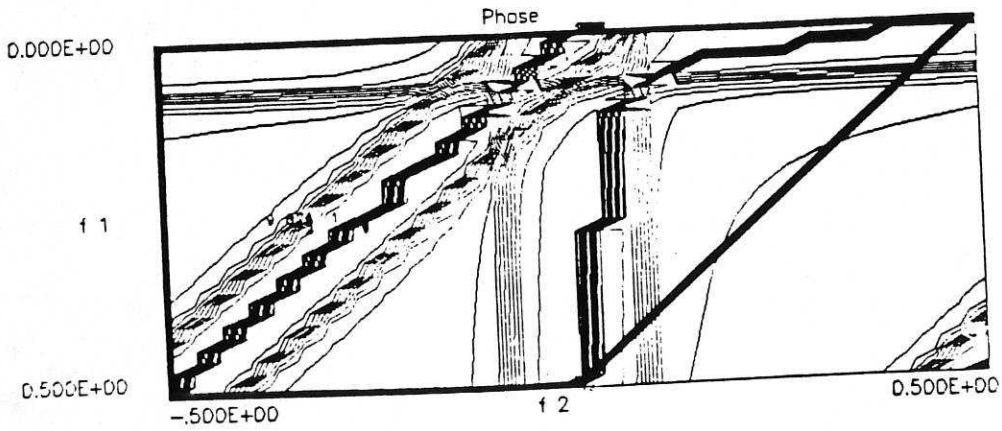
Phase
0.000E+00
f 1
0.500E+00
-.500E+00
f 2
0.500E+00

(d)

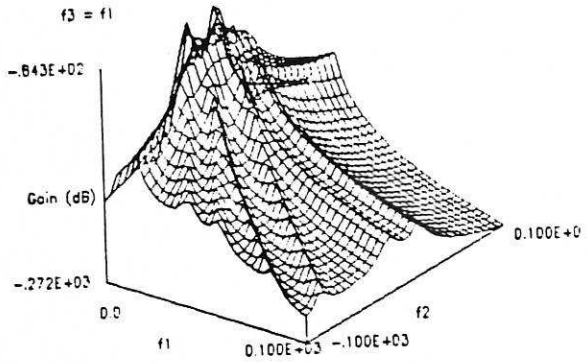
f3 = f1
-.843E+02
Gain (dB)
-.272E+03
0.0
f1
0.100E+03
-.100E+03
f2
0.100E+0

(a)

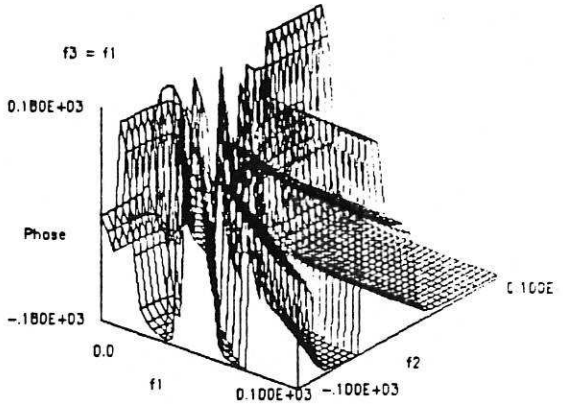
f3 = f1
0.180E+03
Phase
-.180E+03
0.0
f1
0.100E+03
-.100E+03
f2

(b)

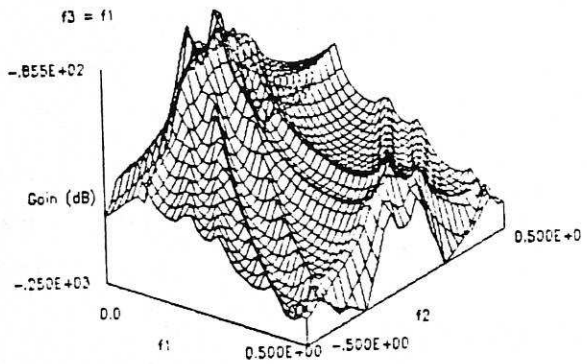
f3 = f1
-.855E+02
Gain (dB)
-.250E+03
0.0
f1
0.500E+00
-.500E+00
f2
0.500E+0

(c)

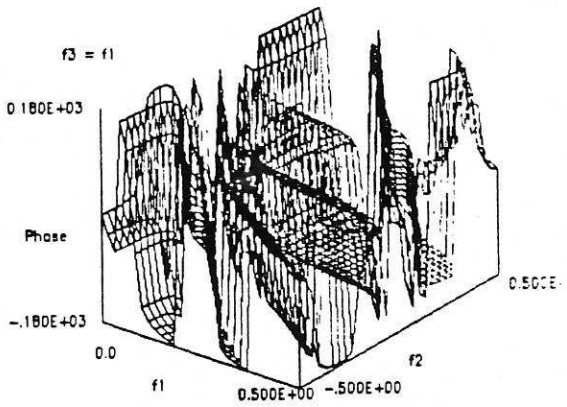
f3 = f1
0.180E+03
Phase
-.180E+03
0.0
f1
0.500E+00
-.500E+00
f2

(d)

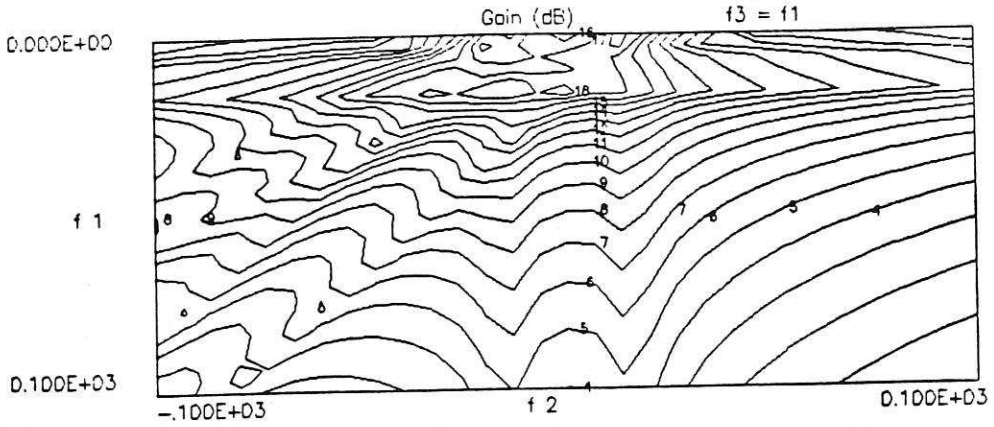
Gain (dB)
f3 = f1
0.000E+00
f 1
0.100E+03
-.100E+03
f 2
0.100E+03

(a)

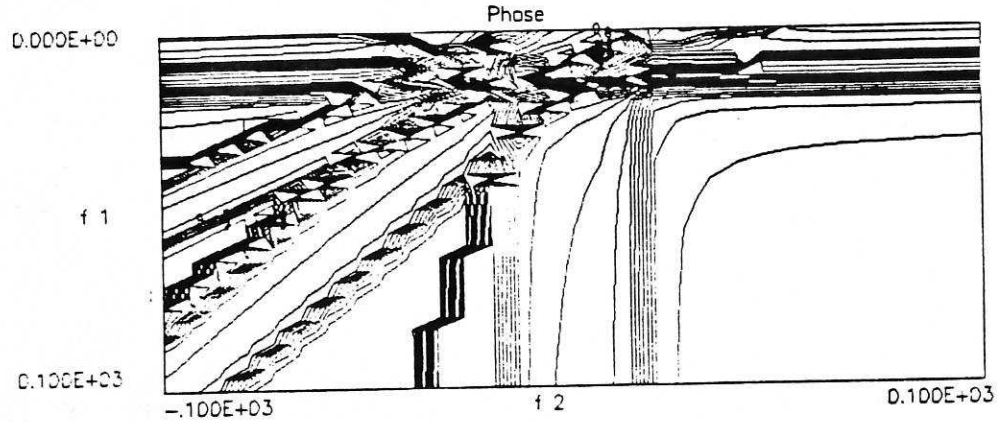
Phase
0.000E+00
f 1
0.100E+03
-.100E+03
f 2
0.100E+03

(b)

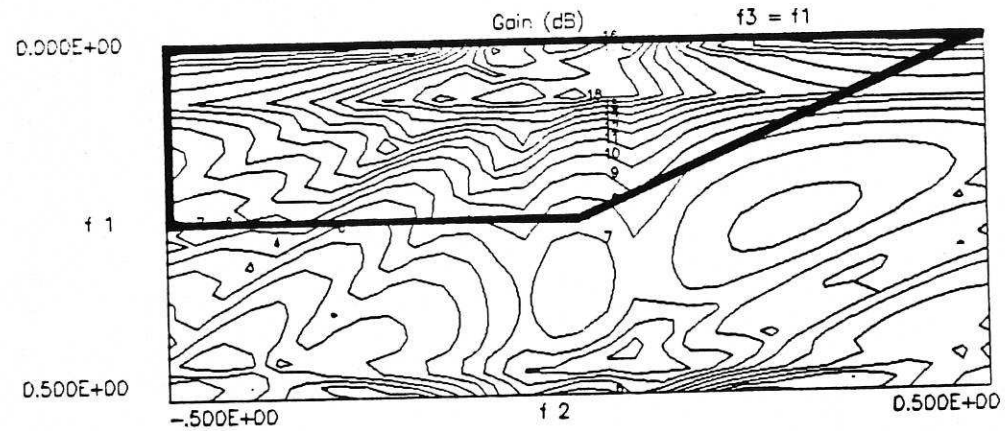
Gain (dB)
f3 = f1
0.000E+00
f 1
0.500E+00
-.500E+00
f 2
0.500E+00

(c)

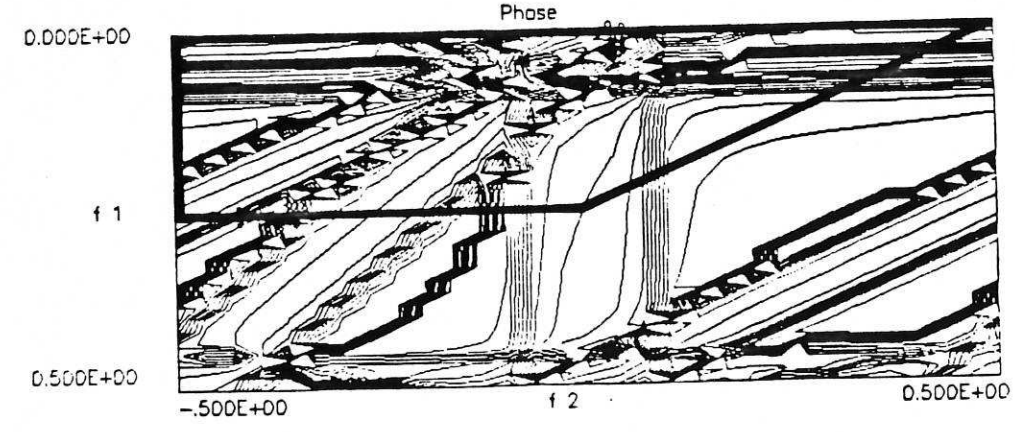
Phase
0.000E+00
f 1
0.500E+00
-.500E+00
f 2
0.500E+00

(d)

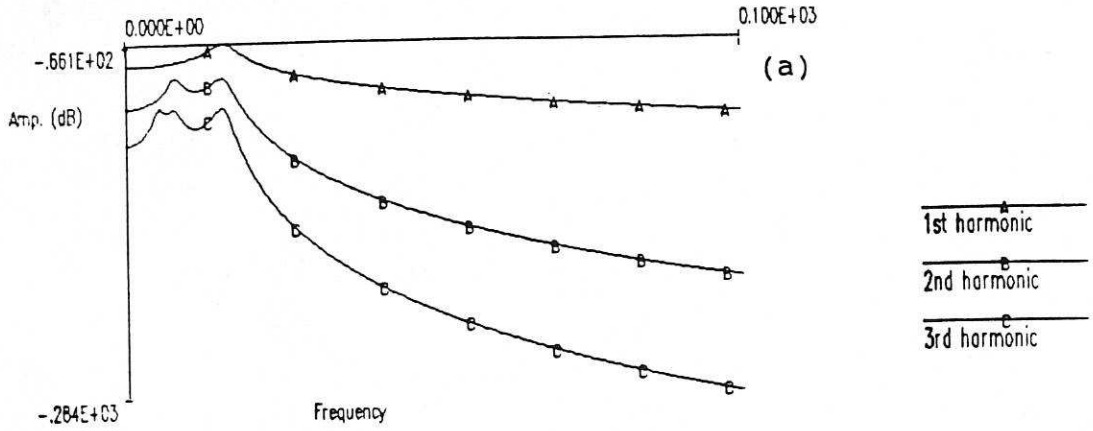
0.000E+00
0.100E+03
-.661E+02
(a)
Amp. (dB)
-.284E+03
Frequency
1st harmonic
2nd harmonic
3rd harmonic

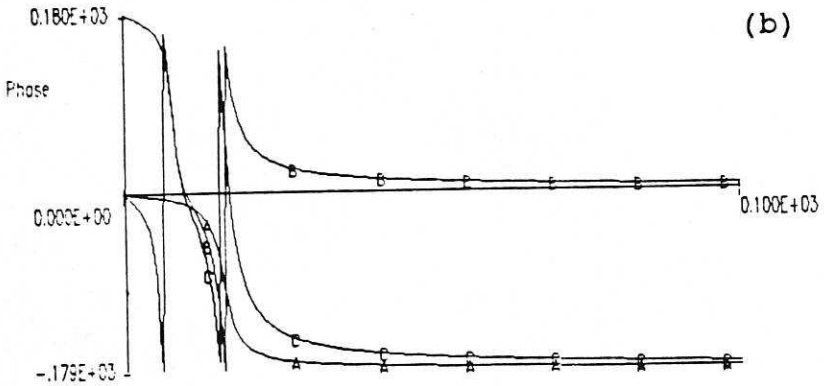
0.180E+03
(b)
Phase
0.000E+00
0.100E+03
-.179E+03

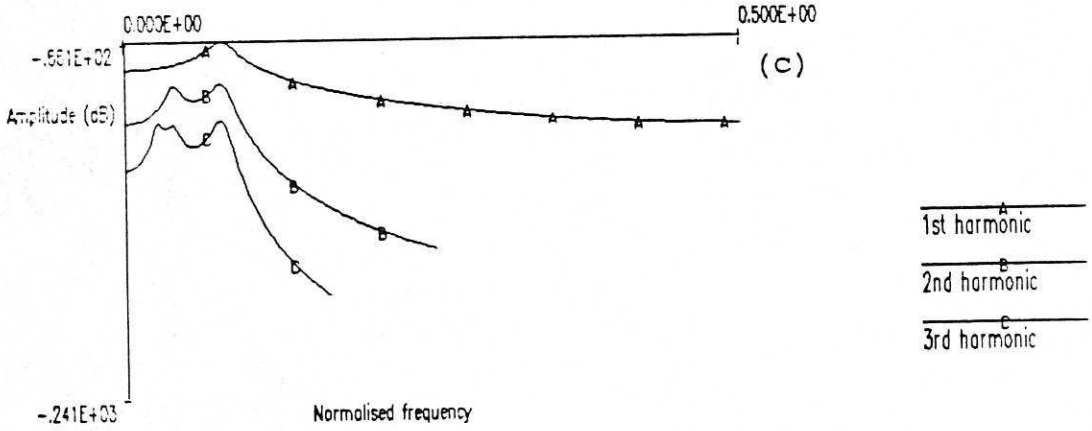
0.000E+00
0.500E+00
-.661E+02
(c)
Amplitude (dB)
-.241E+03
Normalised frequency
1st harmonic
2nd harmonic
3rd harmonic

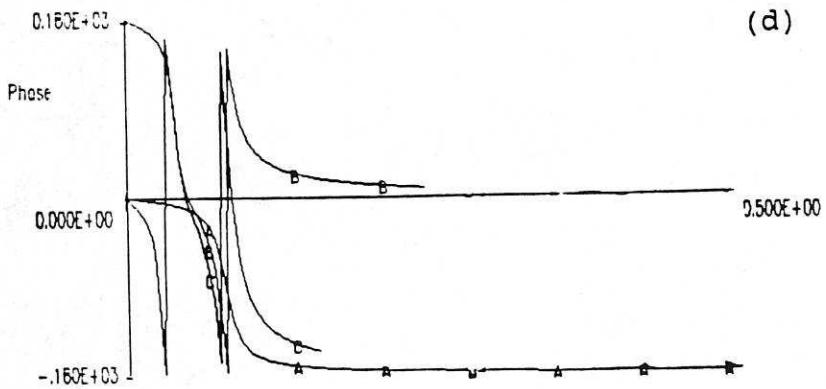
0.180E+03
(d)
Phase
0.000E+00
0.500E+00
-.180E+03

Bode plot - Magnitude

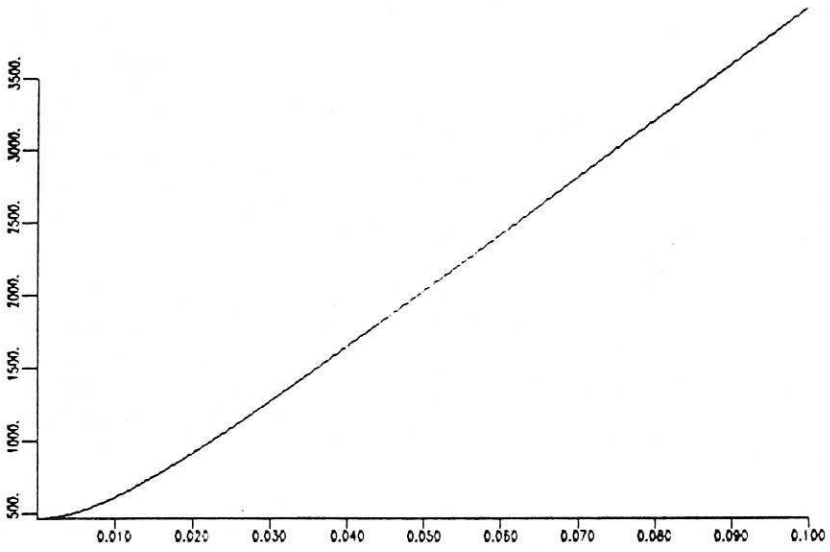

Bode plot - Phase

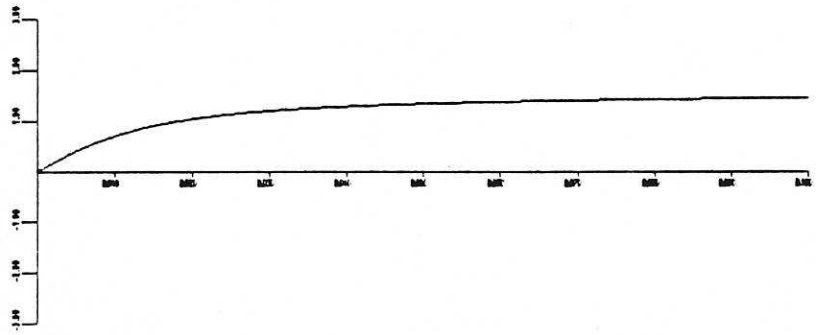

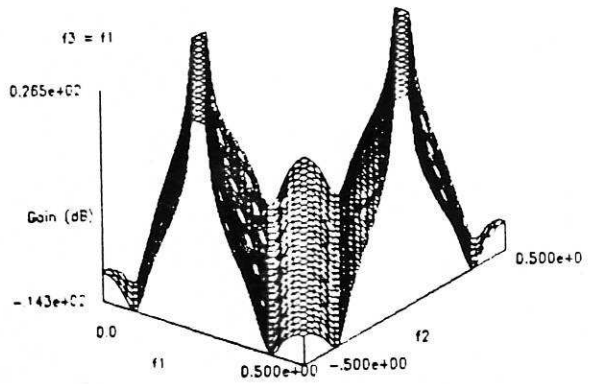
f3 = f1
0.265e+02
Gain (dB)
-.143e+02
0.0
f1
0.500e+00
-.500e+00
f2
0.500e+0

(a)

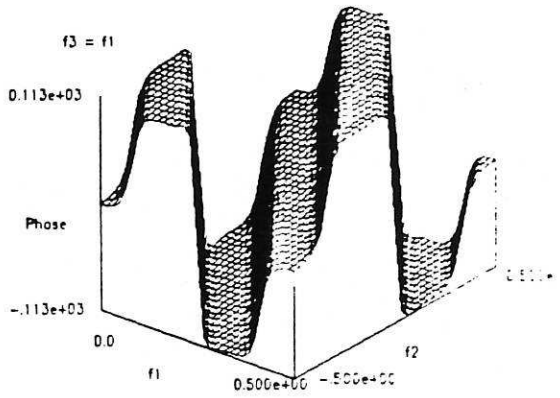
f3 = f1
0.113e+03
Phase
-.113e+03
0.0
f1
0.500e+00
-.500e+00
f2

(b)

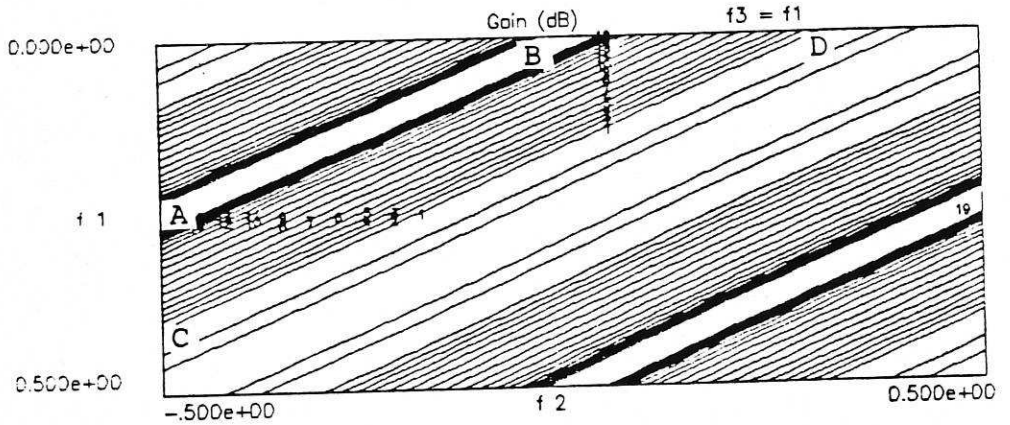
Gain (dB)
f3 = f1
0.000e+00
f 1
0.500e+00
A
B
C
D
19
-.500e+00
f 2
0.500e+00

(c)

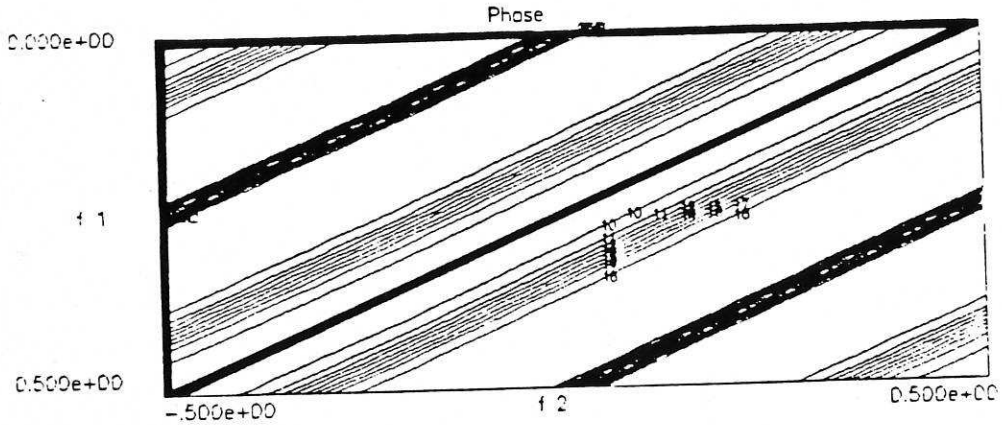
Phase
0.000e+00
f 1
0.500e+00
-.500e+00
f 2
0.500e+00

(d)

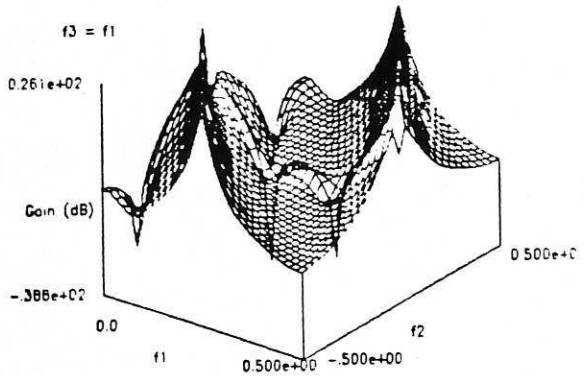
f3 = f1
0.261e+02
Gain (dB)
-.388e+02
0.0
f1
0.500e+00
-.500e+00
f2

(a)

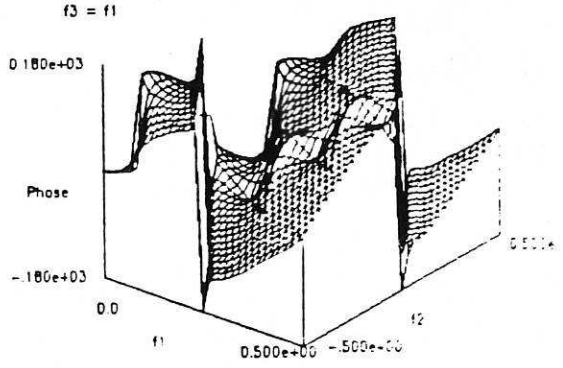
f3 = f1
0.180e+03
Phase
-.180e+03
0.0
f1
0.500e+00
-.500e+00
f2

(b)

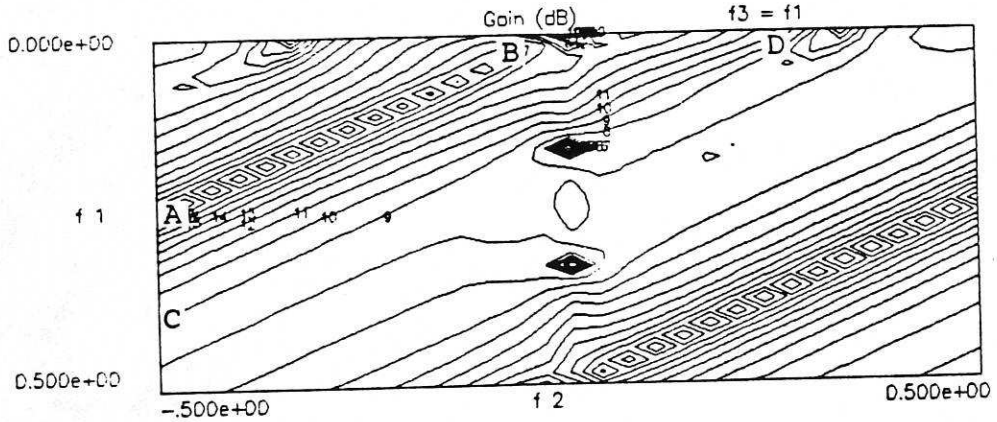
Gain (dB)
f3 = f1
0.000e+00
f 1
0.500e+00
A
B
C
D
-.500e+00
f 2
0.500e+00

(c)

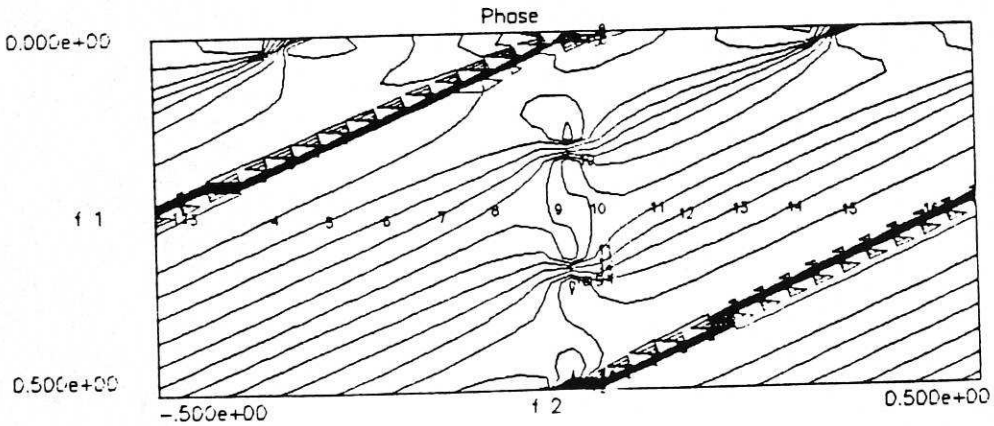
Phase
0.000e+00
f 1
0.500e+00
-.500e+00
f 2
0.500e+00

(d)

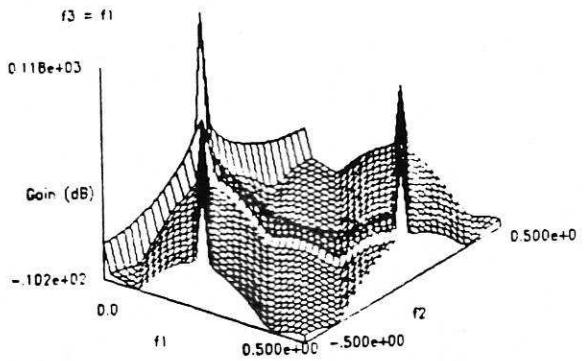
f3 = f1
0.118e+03
Gain (dB)
-.102e+03
0.0
f1
0.500e+00
-.500e+00
f2
0.500e+0

(a)

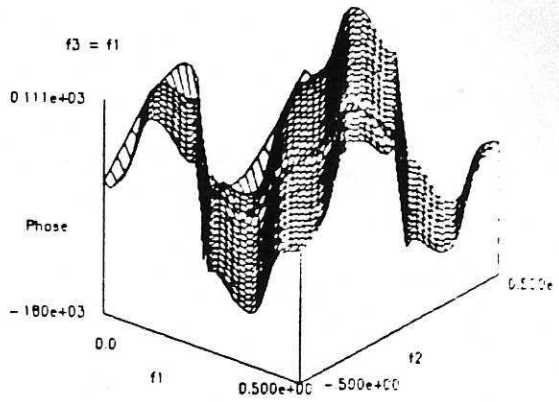
f3 = f1
0.111e+03
Phase
-.180e+03
0.0
f1
0.500e+00
-.500e+00
f2

(b)

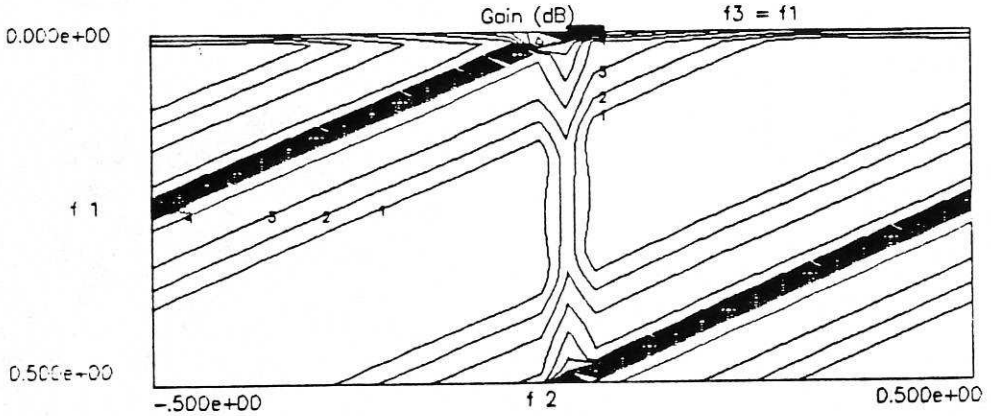
Gain (dB)
f3 = f1
0.000e+00
f 1
0.500e+00
-.500e+00
f 2
0.500e+00

(c)

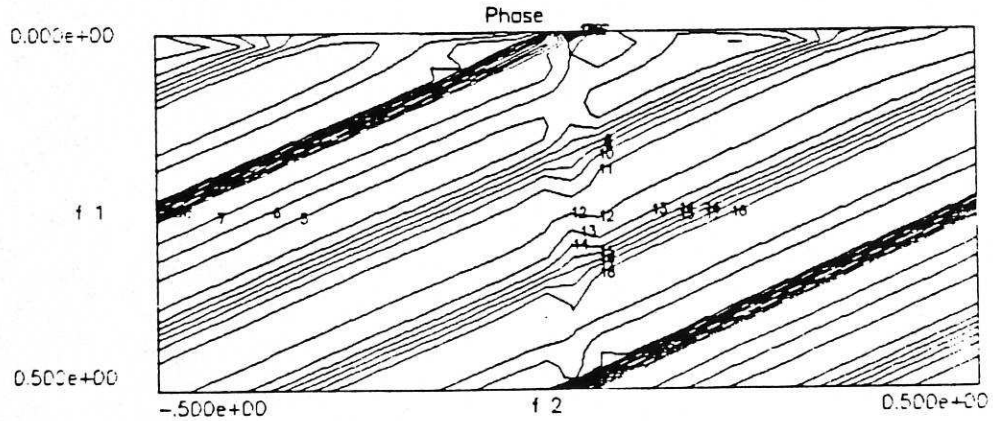
Phase
0.000e+00
f 1
0.500e+00
-.500e+00
f 2
0.500e+00

(d)

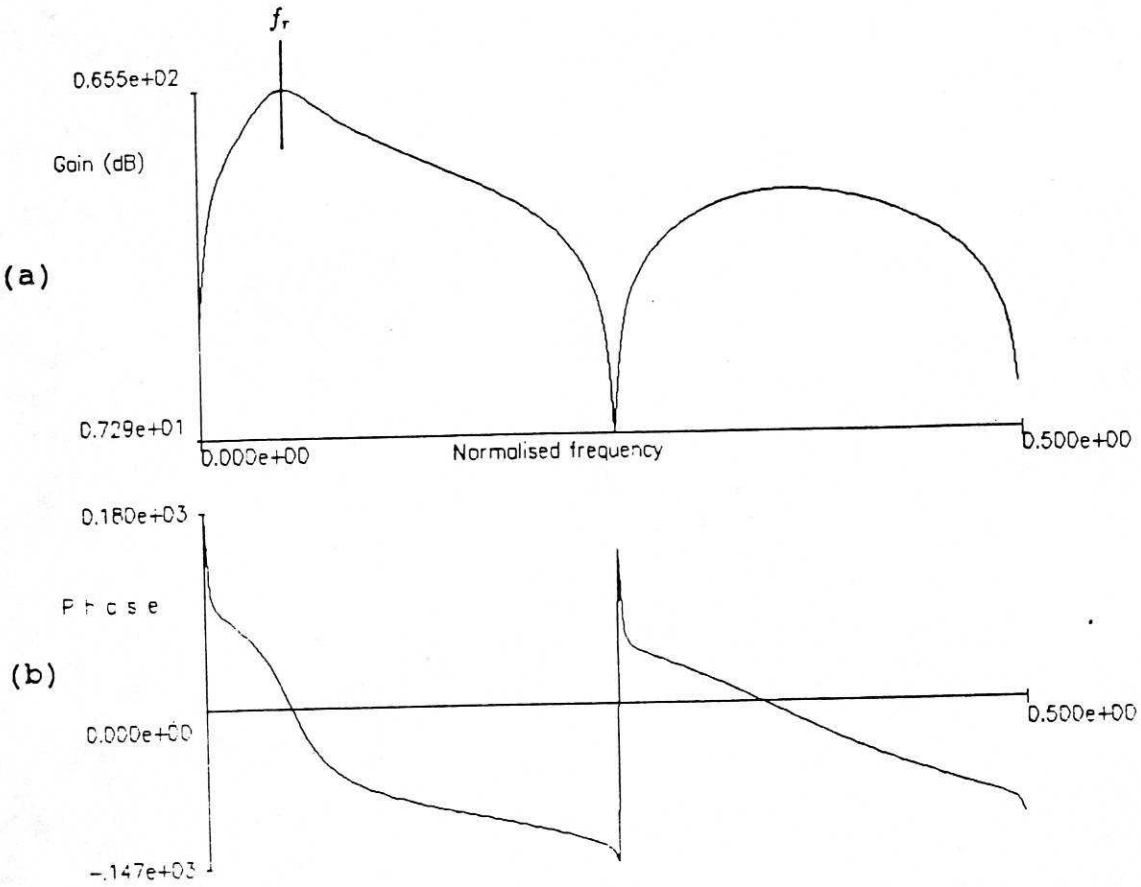
f_r
0.655e+02
Gain (dB)
(a)
0.729e+01
0.000e+00
Normalised frequency
0.500e+00
0.180e+03
Phase
(b)
0.000e+00
0.500e+00
-.147e+03

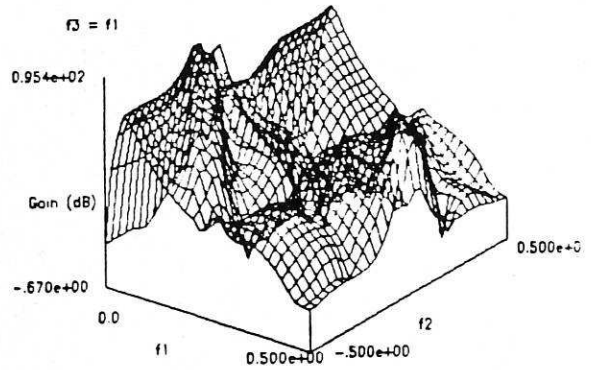
f3 = f1
0.954e+02
Gain (dB)
-.670e+00
0.0
f1
0.500e+00
-.500e+00
f2
0.500e+0

(a)

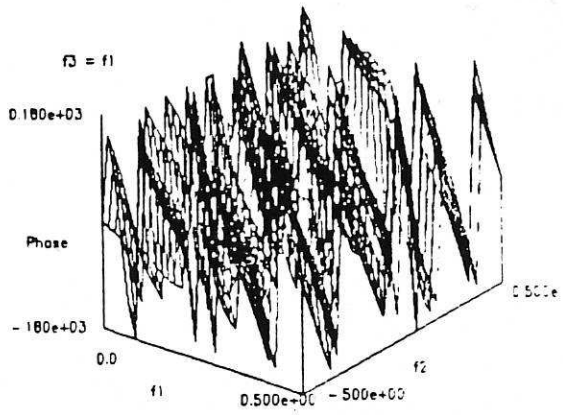
f3 = f1
0.180e+03
Phase
-.180e+03
0.0
f1
0.500e+00
-.500e+00
f2

(b)

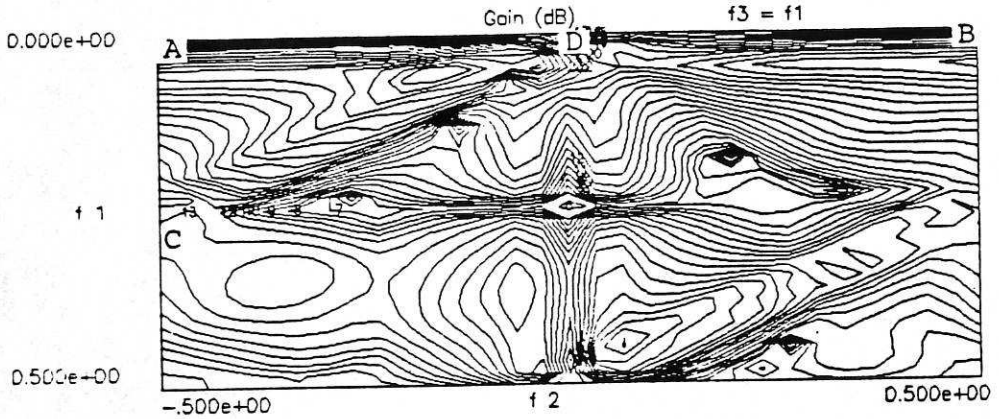
Gain (dB)
f3 = f1
0.000e+00
A
D
B
C
f 1
0.500e+00
-.500e+00
f 2
0.500e+00

(c)

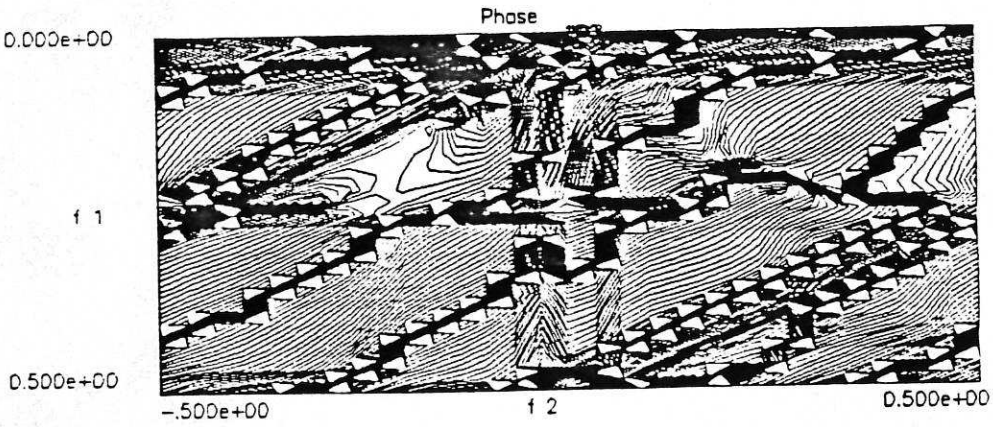
Phase
0.000e+00
f 1
0.500e+00
-.500e+00
f 2
0.500e+00

(d)

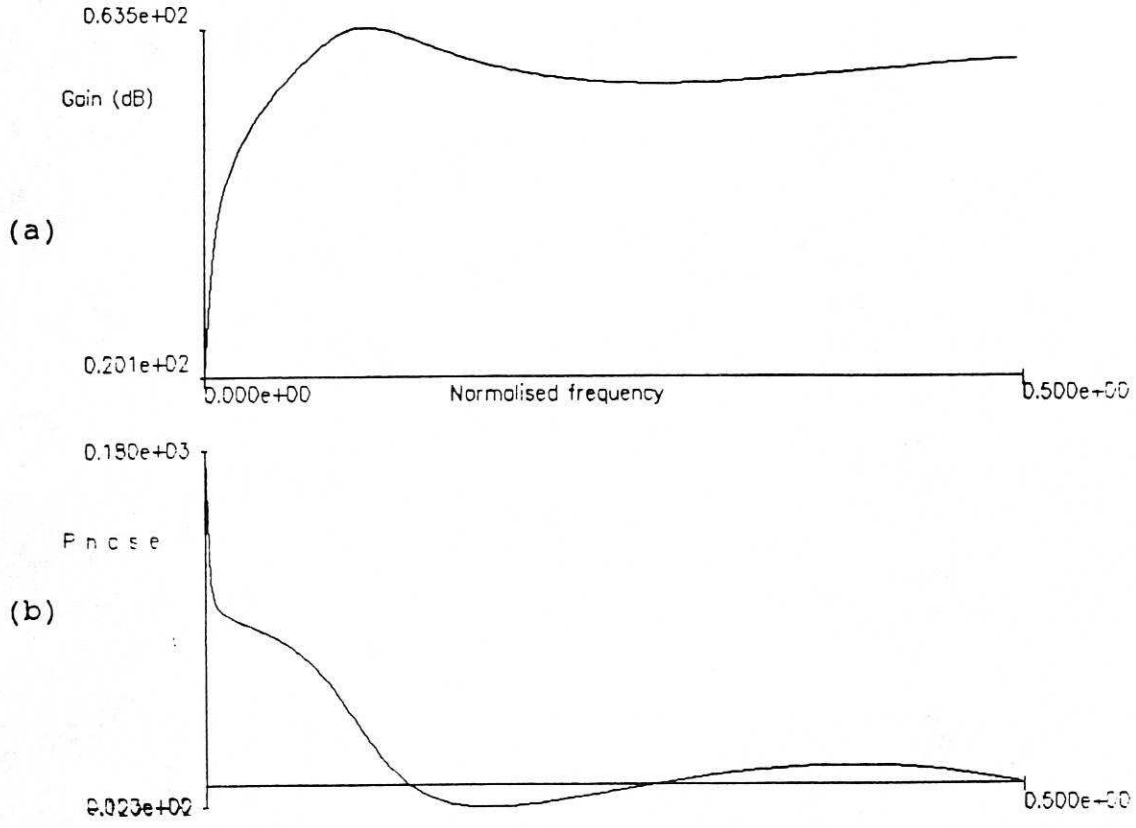
0.635e+02
Gain (dB)
(a)
0.201e+02
0.000e+00
Normalised frequency
0.500e+00
0.180e+03
Phase
(b)
0.023e+02
0.500e+00

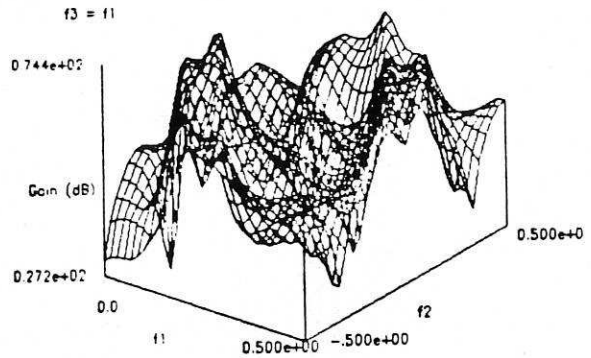
f3 = f1
0.744e+02
Gain (dB)
0.272e+02
0.0
f1
0.500e+00
-.500e+00
f2
0.500e+0

(a)

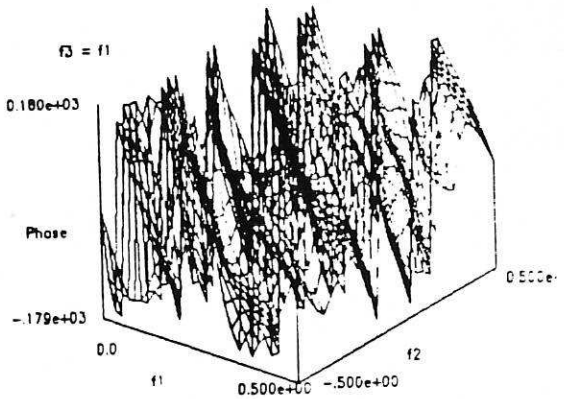
f3 = f1
0.180e+03
Phase
-.179e+03
0.0
f1
0.500e+00
-.500e+00
f2

(b)

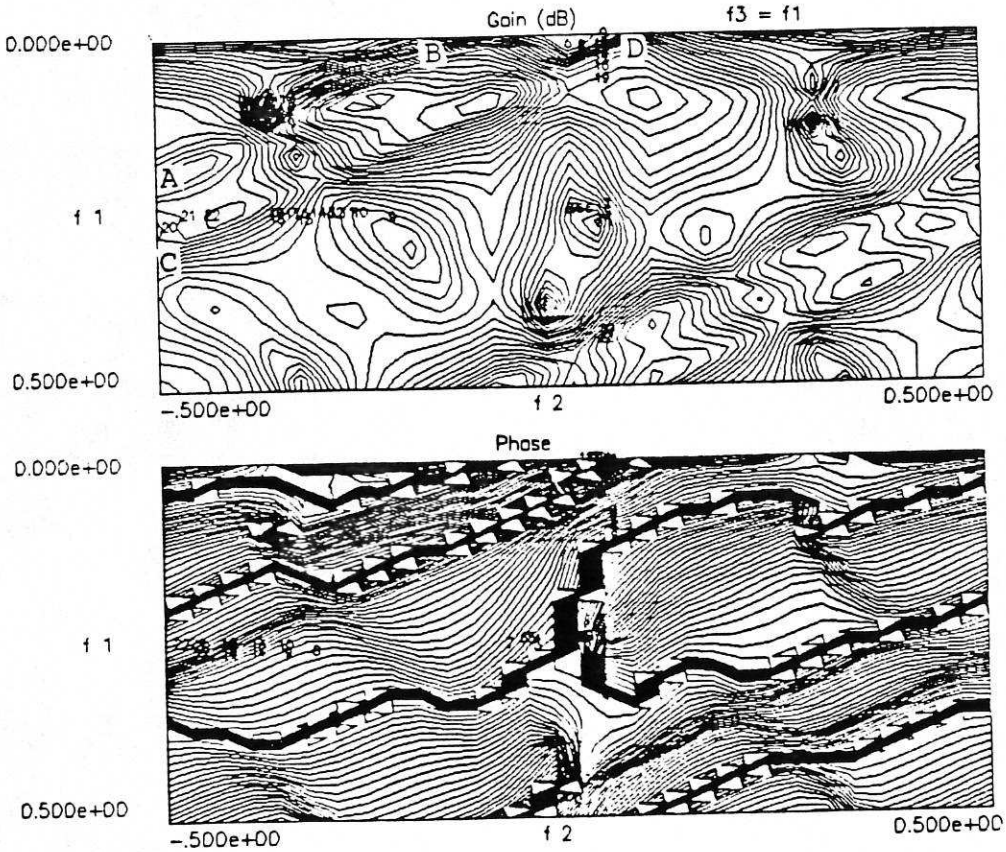
Gain (dB)
f3 = f1
0.000e+00
f 1
0.500e+00
A
B
C
D
-.500e+00
f 2
0.500e+00
Phase
0.000e+00
f 1
0.500e+00
-.500e+00
f 2
0.500e+00

(c)

(d)

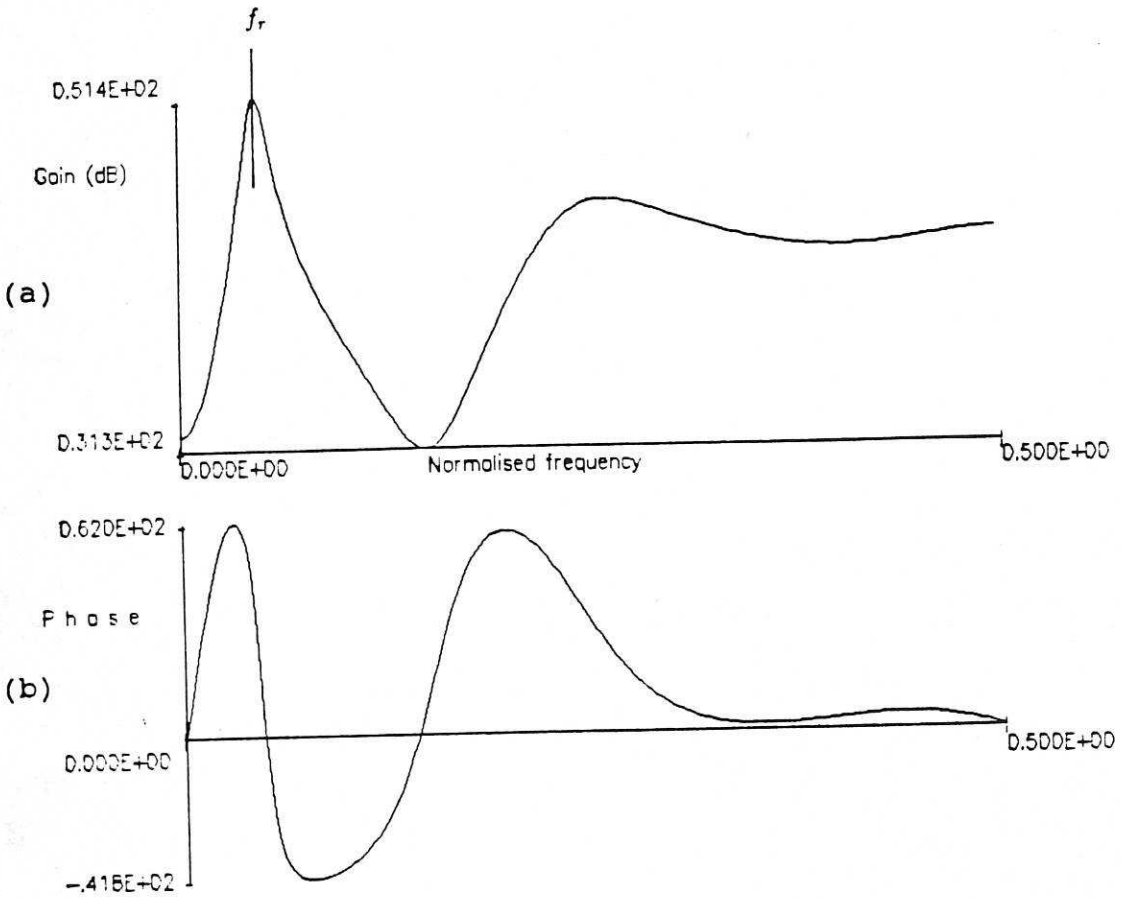
f_r
0.514E+02
Gain (dB)
(a)
0.313E+02
0.000E+00
Normalised frequency
0.500E+00
0.620E+02
Phase
(b)
0.000E+00
-.415E+02
0.500E+00

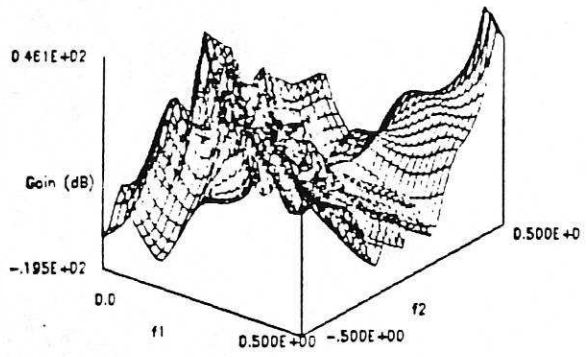
0.4E1E+02
Gain (dB)
-.195E+02
0.0
f1
0.500E+00
-.500E+00
f2
0.500E+0

(a)

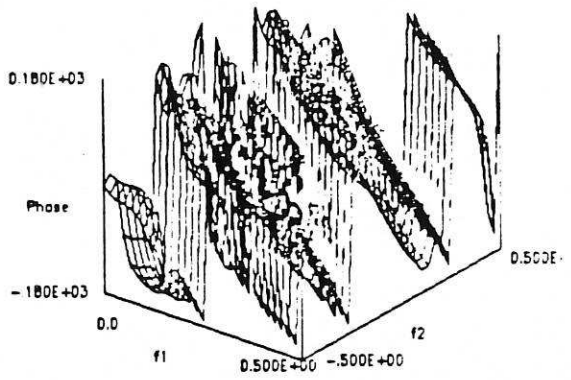
0.1B0E+03
Phase
-.180E+03
0.0
f1
0.500E+00
-.500E+00
f2
0.500E

(b)

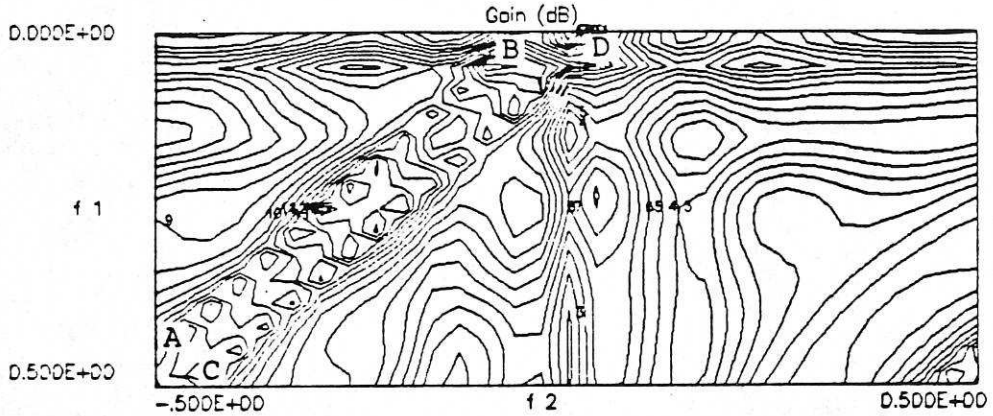
Gain (dB)
0.000E+00
f 1
0.500E+00
B
D
A
C
-.500E+00
f 2
0.500E+00

(c)

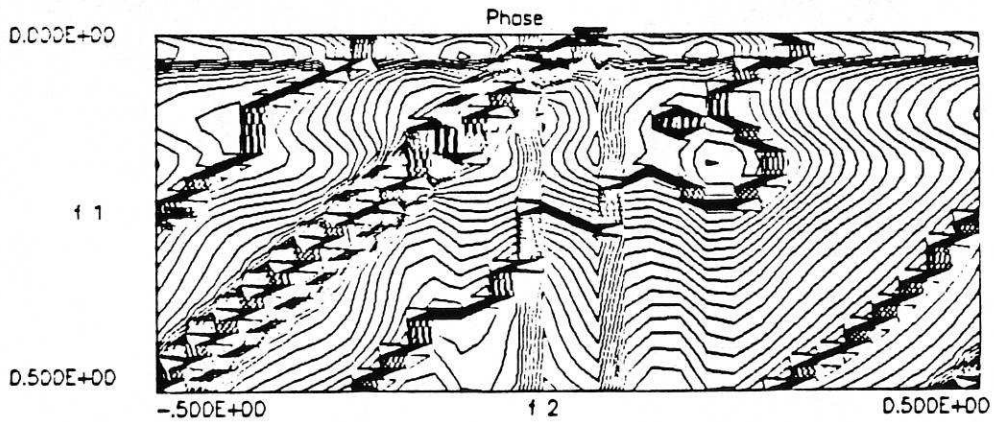
Phase
0.000E+00
f 1
0.500E+00
-.500E+00
f 2
0.500E+00

(d)